J. Fluid Mech. (1997), *vol.* 336, *pp.* 151–182

Subgrid-scale modelling for the large-eddy simulation of high-Reynolds-number boundary layers

By BRANKO KOSOVIĆ

Program in Atmospheric and Oceanic Sciences, Campus Box 429, University of Colorado, Boulder, CO 80309, USA

(Received 25 January 1996 in revised form 6 September 1996)

It has been recognized that the subgrid-scale (SGS) parameterization represents a critical component of a successful large-eddy simulation (LES). Commonly used linear SGS models produce erroneous mean velocity profiles in LES of high-Reynolds-number boundary layer flows. Although recently proposed approaches to solving this problem have resulted in significant improvements, questions about the true nature of the SGS problem in shear-driven high-Reynolds-number flows remain open.

We argue that the SGS models must capture inertial transfer effects including backscatter of energy as well as its redistribution among the normal SGS stress components. These effects are the consequence of nonlinear interactions and anisotropy. In our modelling procedure we adopt a phenomenological approach whereby the SGS stresses are related to the resolved velocity gradients. We show that since the SGS stress tensor is not frame indifferent a more general nonlinear model can be applied to the SGS parameterization. We develop a nonlinear SGS model capable of reproducing the effects of SGS anisotropy characteristic for shear-driven boundary layers. The results obtained using the nonlinear model for the LES of a neutral shear-driven atmospheric boundary layer show a significant improvement in prediction of the non-dimensional shear and low-order statistics compared to the linear Smagorinsky-type models. These results also demonstrate a profound effect of the SGS model on the flow structures.

1. Introduction

Numerical simulation of turbulent flows represents an important research tool in the studies of turbulence phenomena. Three-dimensional numerical simulations of turbulent flows are usually classified as direct Navier–Stokes simulations (DNS) and large-eddy simulations (LES). In a DNS all relevant scales of motions are numerically resolved and therefore a detailed representation of a turbulent flow field can be obtained. The integral-scale Reynolds number is directly proportional to the range of scales in the flow. Therefore, due to the limitations of the present-day computers, DNS is limited to the flows characterized by relatively low Reynolds numbers that do not exceed 10^3. At such low Reynolds numbers the scaling regime of turbulence cannot be reached and therefore the Reynolds-number-independence hypothesis cannot be invoked. While low Reynolds numbers are characteristic for many different flows encountered in engineering applications, turbulent flows in the atmosphere are characterized by Reynolds numbers that are orders of magnitude

greater. A typical value for flow in an atmospheric boundary layer is 10^8. The range of scales in such a flow are far beyond the computational capabilities of present-day computers. The alternative to DNS is LES. In LES, only large energy-containing eddies are numerically resolved. This is accomplished by filtering-out the high-frequency component of the flow field and using the low-pass-filtered form of the Navier–Stokes equations to solve for the large-scale component only. The effects of the filtered-out small-scale fields on the resolved fields are accounted for through the so-called subgrid-scale (SGS) model. The SGS model represents the effects of the interactions between the resolved and unresolved component of the flow field. SGS parameterizations are necessarily based on simplifying assumptions and phenomenological theories and therefore represent the main source of uncertainties and errors in LES.

A critical review of the development of LES and related SGS models has recently been presented by Mason (1994), where he lays out the basic requirements that should be satisfied by a successful LES. Although it cannot provide detailed information about all the scales in the turbulent flow field, LES should result in correct low-order statistics of the flow and mean profiles of the velocity, temperature or any other passive or active scalars advected by the flow field. In addition it should give accurate turbulent stresses and fluxes of related variables, thus providing important information about the turbulent transport and the global features of the flow. Furthermore we expect LES to accurately reproduce the main spectral characteristics of the resolved component of the flow field. However, the first LES of turbulent channel flows (Deardorff 1970; Schumann 1975) showed that even obtaining correct mean velocity profiles cannot be guaranteed. Their LES resulted in an excessive shear in near-wall regions of the flow. Deardorff found that the velocity profile is sensitive to the exact values of the SGS model parameters. Schumann went a step further and in order to correct the errors added a new term to the SGS model. Since the additional term could be viewed as a Reynolds stress model, the actual LES represented a combination of a Reynolds-averaged model near the walls of the channel and a true LES in the interior of the flow field. Successful LES of moderate-Reynolds-number boundary layer flows (Moin & Kim 1982) and convective atmospheric boundary layers (Moeng 1984), outweigh the early problems.

Recently Mason & Thomson (1992) revisited the problem and developed the stochastic backscatter SGS model. Their work was followed by Sullivan, McWilliams & Moeng (1994), who used a modification of Schumann's (1975) model to correct erroneous velocity profiles. Both groups recognized that the intrinsic complexities of inhomogeneous turbulence near the bounding surfaces was reflected in anisotropy due to the shear and the role of the reverse flow of turbulent kinetic energy (TKE). However, in the attempt to develop a better SGS parameterization these two groups took different paths. Mason & Thomson (1992) focused their attention on the features of the energy transfer in LES characterized by an under-resolved energy production in the surface layer and pointed out the necessity of accounting for the flow of energy from the small, unresolved scales of motion toward large, resolved scales by implementing stochastic backscatter of energy. Such an approach was previously suggested by Leith (1990) for a plane shear mixing layer. Sullivan *et al.* (1994) argued that since the flow field near the rigid boundary is under-resolved, it is justified to adopt the Reynolds stress approach in the surface region. They combined the eddy-viscosity model (zeroth-order model) for the mean resolved turbulent stress and the SGS kinetic energy version (Lilly 1967) of the linear SGS model. They chose the anisotropy factor as a weighting parameter to assure a smooth transition between

two models. The fact that the same goal – correct mean velocity profiles – can be achieved using two different approaches prompts a detailed analysis of the SGS effects in the regions of the flow dominated by shear and therefore characterized by anisotropy.

It follows that the LES produces satisfactory results when the main TKE producing mechanism is well resolved. This is the case in simulations of the convective phenomena or in moderate-Reynolds-number flows. When the eddies contributing to the TKE production mechanism are well resolved then the main role of the SGS component is to drain the proper amount of the energy from the resolved flow field. In those cases the SGS effects are small or even insignificant. However, in inhomogeneous shear-driven flows such as those encountered in the surface layers of atmospheric boundary layers the significant component of the TKE production is not fully resolved. The role of the SGS component in such flows often dominates that of the resolved fields. Therefore we will examine more closely the SGS modelling problem. We undertake this task with a goal of isolating and re-examining the properties of SGS models and develop a new SGS model that would satisfy the aforementioned requirements.

In this paper we present an analysis of the effects of the SGS component. We examine the requirements that an SGS model has to satisfy. We present the development of a nonlinear SGS model and demonstrate its performance in LES of a shear-driven boundary layer. The nonlinear SGS model represents an attempt to address both the effects of anisotropy due to the shear and the role of backscatter of energy in under-resolved flow regions.

2. Subgrid-scale modelling problem

In this section we present the main ideas that shaped the development of LES and provide a critical analysis of the methods and techniques involved in the SGS modelling problem. In our analysis we consider incompressible flows characteristic for atmospheric boundary layers. For such flows the momentum conservation equation for the resolved velocity field in a rotating frame of reference is

$$\frac{\partial \tilde{u}_i^r}{\partial t} + \tilde{u}_j^r \frac{\partial \tilde{u}_i^r}{\partial x_j} = -\frac{1}{\rho}\frac{\partial \tilde{p}^r}{\partial x_i} - \frac{\partial \sigma_{ij}}{\partial x_j} - 2\varepsilon_{ijk}\zeta_j \tilde{u}_k^r. \tag{2.1}$$

Here, ζ is the rotation rate of the non-inertial coordinate system (e.g. Earth's rotation). The continuity equation is

$$\frac{\partial \tilde{u}_i^r}{\partial x_i} = 0. \tag{2.2}$$

Assuming neutrally buoyant conditions, we have neglected buoyancy effects that can otherwise be accounted for via the Boussinesq approximation. In the equations (2.1) and (2.2) superscript r denotes resolved fields obtained by filtering total fields so that any filtered field $\tilde{f}^r$ is defined as

$$\tilde{f}^r(\boldsymbol{x}) = \int_{\mathscr{V}} G(\boldsymbol{x} - \boldsymbol{\xi})\, \tilde{f}(\boldsymbol{\xi}) \mathrm{d}\boldsymbol{\xi}. \tag{2.3}$$

Here, $G(\boldsymbol{x})$ is a filter function. In equation (2.1) σ_{ij} is the anisotropic component of the SGS stress tensor τ_{ij}:

$$\sigma_{ij} = \tau_{ij} - \tfrac{1}{3}\tau_{kk}. \tag{2.4}$$

The SGS stress τ_{ij} is defined as

$$\tau_{ij} = (\tilde{u}_i\tilde{u}_j)^r - \tilde{u}_i^r\tilde{u}_j^r$$
$$= (\tilde{u}_i^r\tilde{u}_j^r)^r - \tilde{u}_i^r\tilde{u}_j^r + \left[(\tilde{u}_i^r\tilde{u}_j^s + \tilde{u}_i^s\tilde{u}_j^r) + \tilde{u}_i^s\tilde{u}_j^s\right]^r. \tag{2.5}$$

The isotropic component of the SGS stress $\frac{1}{3}\tau_{kk}$ is added to the pressure $\tilde{p}^r$. In equation (2.5) the superscript s denotes the subgrid fields defined as the difference between the total and filtered fields:

$$\tilde{u}_i^s = \tilde{u}_i - \tilde{u}_i^r. \tag{2.6}$$

To close the system of partial differential equations (2.1) and (2.2) and solve for the resolved velocity we need additional equations for the resolved pressure field and the SGS stresses. The pressure field can be determined from the Poisson equation obtained by taking the divergence of the momentum conservation equation (2.1).

The fundamental question of LES is whether it is possible to express the anisotropic SGS stresses as a functional of the resolved fields. The theory of inertial manifolds (Foias, Manley & Temam 1988) provides a mathematically rigorous framework for constructing closures for systems of partial differential equations truncated in function space. While an approximate inertial manifold can be constructed for the two-dimensional Navier–Stokes system (Foias, Manley & Temam 1991), the extension to a three-dimensional case has not been accomplished yet. Therefore we have to resort to modelling SGS terms using either statistical or phenomenological theories. In general when developing a SGS model we have to assume that any external forcing is either resolved in our simulation or its subgrid component is negligible. Any forcing that has a significant subgrid component can render rational SGS modelling impossible due to the unpredictable effects it can have on the energy transfer between resolved and subgrid eddies.

The foundations of SGS modelling are usually tied to the work of Smagorinsky (1963). He used an eddy-viscosity gradient-diffusion concept to model the SGS effects in a global circulation model. The eddy-viscosity gradient-diffusion concept was first conceived by Boussinesq (1877) and has been extensively used in the framework of Reynolds-averaged Navier–Stokes equations, which can be viewed as a limiting case of the filtered Navier–Stokes equations (2.1) if the ensemble average is approximated by the volume average as is commonly done and the filter $G(\boldsymbol{x})$ becomes a volume average operator, $1/\mathscr{V}$. In this limit the SGS stress given by equation (2.5) reduces to the Reynolds stress

$$\tau_{ij}\Big|_{G=1/\mathscr{V}} = \left[\tilde{u}_i^s\tilde{u}_j^s\right]^r\Big|_{G=1/\mathscr{V}} = \langle u_iu_j\rangle = R_{ij}. \tag{2.7}$$

Here, V is the volume of the flow domain while angle brackets represent an ensemble average approximated by a volume or time average. The fluctuating component of the velocity is

$$u_i = \tilde{u}_i - \langle\tilde{u}_i\rangle. \tag{2.8}$$

Lilly (1966, 1967) developed two different models for the SGS effects in LES. The first model was based on the assumption that the turbulence under consideration has reached the equilibrium state in which production is balanced by dissipation and the inertial range is developed instantaneously. The anisotropic component of the SGS stress is linearly related to the rate of strain:

$$\sigma_{ij} = -2\nu_e S_{ij}. \tag{2.9}$$

Here S_{ij} is strain rate tensor defined as

$$S_{ij} = \frac{1}{2}\left(\frac{\partial \tilde{u}_i^r}{\partial x_j} + \frac{\partial \tilde{u}_j^r}{\partial x_i}\right). \tag{2.10}$$

Now the modelling problem reduces to determining the appropriate eddy viscosity v_e. The model has to be dimensionally consistent. Following the mixing-length concept of Prandtl (1925), Smagorinsky (1963) related the local eddy viscosity to the local rate of strain magnitude

$$v_e = (C_s l)^2 (2S_{kl}S_{lk})^{1/2}. \tag{2.11}$$

Here l is the characteristic length scale and C_s is the Smagorinsky constant. Lilly designed a different model for the turbulence in which an equilibrium range is not developed instantaneously. This is usually the case in highly inhomogeneous flows. For the subgrid-scale eddy-viscosity coefficient, Lilly adopted Prandtl's modified eddy-viscosity relation whereby the eddy-viscosity coefficient is related to the product of a characteristic length scale (the grid-cell size) and a characteristic velocity scale (the square root of the turbulent kinetic energy)

$$v_e = C_e l\ (e_{sgs}^r)^{1/2}. \tag{2.12}$$

In this case, an additional partial differential equation for the SGS kinetic energy is solved along with the Navier–Stokes equations:

$$\frac{\partial e_{sgs}^r}{\partial t} + \left[u_j^r \frac{\partial e_{sgs}^r}{\partial x_j}\right]^r = -\tau_{ij}\frac{\partial u_i^r}{\partial x_j} - \frac{\partial\left[u_i^s(e_{sgs} + p^s/\rho)\right]^r}{\partial x_i} - \epsilon. \tag{2.13}$$

The SGS turbulent kinetic energy e_{sgs} is defined as

$$e_{sgs} = \tfrac{1}{2}\left[(\tilde{u}_l\tilde{u}_l)^r - \tilde{u}_l^r\tilde{u}_l^r\right]. \tag{2.14}$$

In equation (2.13) ϵ denotes the dissipation rate which has to be modelled along with the transport term (the second term on the right-hand side of the equation). For both models, Lilly analytically determined the model constants, which he considered to be universal. The first model (2.11) is now usually referred to as the Smagorinsky model while Lilly labelled the second model (2.12) the "turbulent energy model". Following the nomenclature used in Reynolds stress modelling, the turbulent energy model would be equivalent to the one-equation closure where only one additional prognostic equation for the TKE is solved along with the original system of equations. We should point out that most of the work on LES and SGS modelling that followed has roots in Lilly's early work and its foundations: the Kolmogorov inertial-range hypothesis, the notion of an eddy viscosity, and Prandtl's mixing length theory. Following the terminology of the constitutive theory we label the model defined by equations (2.9) and (2.11) or (2.12) a linear model since on a tensor level it linearly relates the SGS stress tensor to the strain rate tensor with an eddy viscosity as a proportionality parameter. The adoption of such a simple model for SGS stresses in LES is justified by the assumption that the local SGS effects cannot significantly affect the resolved velocity field and that only global energy transfer has to be accurately represented by the model.

The parameters in Boussinesq eddy-viscosity-based models are adjusted to satisfy global energy balances. Such models predict only the net energy transfer from large scales to small scales. However, DNS results have confirmed that the local inverse transfer of energy is possible (e.g. Domaradzki, Liu & Brachet 1993). The backscatter of energy can be associated with the formation of the large coherent structures in the

flow field. Mason & Thompson (1992) introduced stochastic backscatter effects in their SGS model. They argued that the stochastic fluctuations of the SGS stress divergence and their correlation with the resolved velocity field are essential for obtaining correct low-order turbulent statistics using LES. Recently Piomelli, Yunfang & Adrian (1996) studied the SGS energy transfer and associated structures in low-Reynolds-number wall-bounded flows. They found that in the logarithmic region of the boundary layer both forward and backward energy transfer are associated with events known as ejections where the low-momentum fluid from the near-wall region is ejected into the inner region of the boundary layer. Piomelli *et al.* (1996) therefore argued that the stochastic backscatter model alone is not sufficient since it cannot account for the deterministic structures in the near-wall region.

In the following sections we focus on problems related to the LES of high-Reynolds-number boundary layer flows. More specifically we attempt to find an explanation for the erroneous velocity profiles observed in the LES of atmospheric boundary layers and offer a possible solution to that problem. In the first LES of high-Reynolds-number channel flow performed by Deardorff (1970), he noticed that the mean velocity profiles did not follow experimental observations. His LES could not accurately reproduce the logarithmic layer. Later, Schumann (1975) confirmed that LES consistently over-predicted the mean velocity magnitudes and consequently mean wind shear.

In our analysis we assume that the filter used is a wave cut-off filter in two homogeneous directions. In the inhomogeneous direction normal to the solid boundary, no explicit filters are applied. The wave cut-off filter gives resolved and subgrid fields that are uncorrelated.

The LES results obtained using linear SGS models show that the ensemble-average tangential turbulent stresses (total as well as resolved) are accurately reproduced. This may be explained by the fact that the mean tangential stresses have to satisfy the mean momentum equations of the form

$$\frac{\partial(\langle u_1^r u_3^r\rangle + \langle\sigma_{13}\rangle)}{\partial x_3} = f(U_2 - U_{g2}) \quad \text{and} \quad \frac{\partial(\langle u_2^r u_3^r\rangle + \langle\sigma_{23}\rangle)}{\partial x_3} = -f(U_1 - U_{g1}). \quad (2.15)$$

Here, f is the Coriolis parameter ($f = 2\zeta \sin\phi$, where ϕ is the latitude), while U_{gj} is the jth component of the geostrophic wind. A relation similar to (2.15) can be written for the normal SGS stress component $\langle u_3^r u_3^r\rangle + \langle\sigma_{33}\rangle$. In flows driven by a mean pressure gradient, a similar relation exists. These simple relations ensure that the total turbulent stress profiles obtained are correct. No such relation exists involving the mean normal SGS stress components $\langle\sigma_{11}\rangle$ and $\langle\sigma_{22}\rangle$ or tangential component $\langle\sigma_{12}\rangle$.

By analogy with the ensemble-mean streamwise velocity variance equation for horizontally homogeneous turbulent flows, we can write the conservation equation for the corresponding component of the resolved turbulent stress $u_1^r u_1^r$. Assuming that the x-coordinate is aligned with the mean wind in the surface layer it follows that

$$\langle u_1^r u_3^r\rangle \frac{\partial U_1}{\partial x_3} = -\frac{1}{2}\frac{\partial\langle u_1^r u_1^r u_3^r\rangle}{\partial x_3} - \frac{1}{\rho}\left\langle u_1^r \frac{\partial p^r}{\partial x_1}\right\rangle - \left\langle u_1^r \frac{\partial(\sigma_{1j} - \langle\sigma_{1j}\rangle)}{\partial x_j}\right\rangle. \quad (2.16)$$

Here u_i^r, p^r, are fluctuating components of the resolved velocity and pressure fields. Equation (2.16) is the lowest-order equation that relates the mean shear to the SGS stress. If the resolved tangential turbulent stress in an LES is accurately represented then we can conclude that only the fluctuating component of the SGS stresses and their correlation with the resolved velocity field can directly affect the mean

velocity profile through (2.16). The fluctuating component of the SGS stress therefore represents a possible cause of erroneous mean wind profiles.

3. Constitutive theory and the SGS modelling problem

From the first attempts by Boussinesq to the present phenomenological turbulence, modelling has followed the ideas of constitutive theories for viscous stresses in fluids. Seeking the proper turbulence model in the framework of models for molecular diffusion was motivated by observations which showed that turbulence enhances mixing and diffusion of momentum, temperature and passive scalars. The effort to develop more effective models for turbulent stresses has long focused on defining a proper eddy-viscosity coefficient, in spite of the evidence that the gradient diffusion itself cannot account for some important phenomena observed in turbulence. Boussinesq eddy-viscosity models cannot account for the normal stress effects (Lumley 1970) and unless negative eddy viscosities are allowed (Germano *et al.* 1991; Piomelli *et al.* 1991) they are absolutely dissipative. Absolute dissipation is in contradiction with the fact that the inertial transfer of energy can result in a local backscatter of energy where subgrid effects are the source of the resolved TKE.

The modelling procedure for the Newtonian (linear) fluids was introduced by Stokes in 19th century. A more general and rigorous constitutive theory was developed much later (Rivlin & Ericksen 1955; Coleman & Noll 1960; Truesdell & Noll 1965). Following Truesdell's (1977) development of the constitutive relations for simple fluids (fluids without structure), we list the requirements that should be satisfied by the SGS model.

According to Truesdell (1977), when modelling simple fluids three main principles must be observed: *the principle of determinism*, *the principle of local action*, and *the principle of material frame indifference*. In turbulence modelling adhering to the principle of determinism is often abandoned in favour of the stochastic approach (e.g. Mason & Thomson 1992; Schumann 1995). SGS turbulent fields are the consequence of the evolution of a complex nonlinear dynamical system (cf. Foias *et al.* 1988) and therefore appear random. However, the evolution of SGS fields is governed by deterministic equations forced by their interaction with the deterministic large-scale fields. These interactions can be modelled using the stochastic or the deterministic approach or their combination. We argue that as long as the turbulence production mechanism is known and the production itself is well resolved and can be represented in terms of resolved flow variables, then observing this principle when modelling SGS stresses is justifiable. The principle of local action is sometimes disputed due to the fact that turbulence can result in non-local effects. However, integral forms of constitutive relations that can account for memory effects in materials both satisfy the principle of local action (cf. Truesdell 1977) and are able to reproduce non-local effects observed in turbulent flows. This fact is apparent when we take into consideration sensitivity to initial conditions characteristic for nonlinear dynamical systems. The third principle which implies that the response of the fluid is the same for all observers requires a closer look. The frame indifference is equivalent to the homogeneity and isotropy of the space (not the fluid or the flow) implying that there are no preferred directions or placements in it.

Besides satisfying these three principles, the constitutive relation must be consistent with the general principles of mass conservation, momentum, angular momentum, and energy balance, as well as the second law of thermodynamics (positive, semi-definite entropy). Also, it must be dimensionally consistent. In static equilibrium, a fluid obeys the laws of Eulerian hydrostatics and the stress reduces to the normal

stress only. Furthermore, in the absence of the integral angular momentum, the stress tensor must be symmetric. Due to the symmetry and the material frame indifference requirement the model for the anisotropic component of the viscous stress for simple fluids (often called Reiner–Rivlin fluids) reduces to (Serrin 1959)

$$\Sigma_{ij} = \varpi_1 \, \tilde{S}_{ij} + \varpi_2 \left(\tilde{S}_{ik}\tilde{S}_{kj} - \tfrac{1}{3} \, \tilde{S}_{mn}\tilde{S}_{mn}\delta_{ij} \right). \tag{3.1}$$

Here, Σ_{ij} is the anisotropic viscous stress tensor and $\tilde{S}_{ij}$ is the strain rate tensor based on the total velocity field. The rotation rate tensor does not enter this constitutive relation since it is antisymmetric and tensor products involving the rotation rate tensor are not frame indifferent. The functions ϖ_1 and ϖ_2 are scalar functions of the principal invariants of the rate of strain tensor. Leigh (1962) pointed out that the nonlinear stress component $\tilde{S}_{ik}\tilde{S}_{kj}$ can reproduce the normal stress effects and also result in negative entropy. Therefore the only model which satisfies all the aforementioned constraints including positive definite entropy is the linear model for which $\varpi_2 = 0$. Note that when $\varpi_1 = \nu = f(T)$ the constitutive relation for the Newtonian fluids is recovered, while when $\varpi_1 = \nu_e$ where ν_e is defined by (2.11) Smagorinsky SGS model is obtained.

Rivlin (1957) was the first to suggest that the constitutive theory for nonlinear simple fluids can be used in turbulence modelling. Such a theory can account for the differences in normal viscous stresses and resulting secondary flows in low-Reynolds-number flows in pipes with non-circular cross-sections. When drawing the analogy between the conditions under which normal stress effects are observed in nonlinear high-polymer solutions and turbulent flows, Rivlin conjectured that the turbulent eddies subjected to shear undergo preferential orientation which leads to the observed normal stress effects in turbulent shear flows. The preferential orientation of vortices in sheared turbulent flows was later theoretically explained by a vortex stretching and tilting mechanism (cf. Tennekes & Lumley 1972). The validity of this conceptual picture was confirmed using DNS (Rogers & Moin 1987).

We show that when a constitutive theory is applied to the SGS modelling problem the following requirements can be relaxed: the modelled SGS stress tensor does not have to be frame indifferent and local negative entropy can be allowed. Depending on the type of filter used to split the fields into resolved and SGS components an additional realizability condition must be imposed (Vreman, Geurts & Kuerten 1994). However, since we use a wave cut-off filter this condition does not have to be satisfied.

Lumley (1970) was the first to examine the implications of the constitutive theory for simple fluids (3.1) on turbulence modelling. He presented an *ad hoc* argument showing that frame indifference does not have to be satisfied in turbulence modelling.

Speziale (1985) showed that the SGS stress tensor defined by (2.5) is Galilean invariant, i.e. invariant in all inertial frames of reference and consequently acceptable SGS models must be Galilean invariant. However, it is easy to show (see the Appendix) that the SGS stress does not satisfy frame indifference in rotating frames of reference. Any flow with non-vanishing mean intrinsic vorticity, $\mathscr{W}_i = 2\zeta_i + \langle \tilde{\omega}_i \rangle \neq 0$, can be viewed as a flow in a rotating frame of reference. This implies that SGS models for such flows should not be frame indifferent. The effects of intrinsic vorticity are deterministic and as such justify the deterministic phenomenological approach. As a consequence nonlinear constitutive relations involving the rate of rotation tensor are admissible models for SGS stresses. We therefore argue that a model based on the nonlinear constitutive relation represents a viable choice for LES of boundary layer flows.

Speziale (1981) demonstrated that frame indifference of the Reynolds stress is restored in two-dimensional flows due to the existence of the velocity stream function. In two-dimensional flows we can express the Coriolis term as the gradient of the scalar potential $2\mathscr{W}\psi$, where ψ is the stream function. This scalar potential field can be added to the pressure term and thus the frame indifference of the SGS term is restored. In a three-dimensional flow the Coriolis term cannot be expressed as a gradient of a scalar potential due to non-existence of a stream function. Numerical simulations of isotropic turbulence subjected to rotation showed that the Coriolis effects reduce the TKE dissipation rate (Bardina, Ferziger & Rogallo 1985; Cambon *et al.* 1994). Although in these simulations the normal Reynolds stress components did not exhibit a significant departure from isotropy the reduced inertial transfer of energy affected the redistribution of energy among scales of motion. This redistribution of TKE can be manifested as anisotropic partition of energy among different resolved and SGS normal stress components. In the Appendix we show that Coriolis effects induced by intrinsic vorticity can indeed cause increased anisotropy levels among SGS normal stress components.

Using a reduced form of the constitutive relation for the nonlinear Rivlin–Ericksen (Rivlin 1955) fluids, Pope (1975) developed a general eddy-viscosity hypothesis relating the Reynolds stresses to a finite number of known tensors and scalars which are functions of tensor invariants. In a three-dimensional case, according to Spencer & Rivlin (1959) the Rivlin–Ericksen constitutive relation involves ten independent tensors that are functions of the strain rate tensor and the rotation rate tensor. It also includes five independent invariants. To make the modelling problem analytically tractable, Pope studied the model including only three lowest-order tensors. Only recently were Gatski & Speziale (1993), using the symbolic-algebra software package, able to conduct the analysis of the full Rivlin–Ericksen constitutive relation applied to the Reynolds stress turbulence closure.

Lund & Novikov (1992) performed an *a priori* analysis of the reduced nonlinear constitutive relation involving five lower-order tensors. They used multiregressional analysis to determine most appropriate functional forms for model coefficients. They found that the nonlinear model resulted in higher correlations between actual and modelled SGS stresses. However, when they used constant values of model coefficients the nonlinear model gave only slightly higher correlations as compared to the linear model. Lund & Novikov never used the nonlinear model in an LES. Here we point out that Piomelli, Moin & Ferziger (1988) showed that *a priori* analysis cannot provide detailed quantitative but only qualitative estimates of the SGS model performance.

A general nonlinear constitutive relation similar to that for Rivlin–Ericksen fluids was presented by Speziale (1991) in the following form:

$$\sigma_{ij} = -(C_0 l)^2 \left\{ \frac{1}{\theta_0} S_{ij} \; + C_1 \left(S_{ik} S_{jk} - \tfrac{1}{3}\, S_{mn} S_{mn}\, \delta_{ij} \right) + C_2 \left(S_{ik}\, \Omega_{kj} - \Omega_{ik}\, S_{kj} \right) \right.$$
$$\left. + C_3 \left(\Omega_{ik} \Omega_{kj} - \tfrac{1}{3}\, \Omega_{mn} \Omega_{mn}\, \delta_{ij} \right) + C_4 \left(\frac{\partial S_{ij}}{\partial t} + \tilde{u}_k^r \frac{\partial S_{ij}}{\partial x_j} \right) \right\}. \quad (3.2)$$

Here, θ_0 is the time scale, Ω_{ij} is the rotation rate tensor based on the resolved velocity field, and C_i are model parameters. Speziale (1987) also developed a nonlinear $K-\epsilon$ model based on the frame indifferent form of (3.2). Wong (1992) suggested combining Speziale's nonlinear $K-\epsilon$ model with the Germano *et al.*'s (1991) dynamic SGS model.

Finally, it should be pointed out that nonlinear models were also developed using

formal expansion techniques like direct interaction approximation (Yoshizawa 1984) and the renormalization group (Rubinstein & Barton 1990).

Due to the computational limitations it is not feasible to use the complete Rivlin–Ericksen constitutive relation or relation (3.2) as a model for SGS stresses. We therefore adopt the reduced model and use the same three tensor components as Pope (1975) which are identical to the first three tensor components on the right-hand side of (3.2). We eliminate the fourth term because it yields an erroneous prediction for isotropic turbulence subjected to a solid-body rotation (Gatski & Speziale 1993). The last term may be neglected assuming Taylor's hypothesis, according to which advection of a quantity (in this case the rate of strain) by the mean velocity field is balanced by its time rate of change. It is difficult to justify such an assumption in LES where advection is carried out by resolved velocity fields. However, the computational burden of calculating the material derivative of the strain rate tensor is a prohibitive factor and therefore we discard this term from our model.

The nonlinear model for the SGS stress is defined as

$$\sigma_{ij} = -(C_s\Delta)^2 \left\{ 2(2S_{mn}S_{mn})^{1/2} S_{ij} + C_1 \left(S_{ik}S_{kj} - \tfrac{1}{3}\, S_{mn}S_{mn}\, \delta_{ij} \right) + C_2 \left(S_{ik}\, \Omega_{kj} - \Omega_{ik}\, S_{kj} \right) \right\}. \tag{3.3}$$

Here, C_s is Smagorinsky constant and Δ is a length scale related to the grid-cell size (Moeng 1984). Since we are concerned with inhomogeneous high-Reynolds-number boundary layer flows it is more appropriate to use the SGS TKE equation (2.13) to determine the proper velocity scale for the transport coefficient associated with the linear term. Then the corresponding model based on Lilly's "turbulent energy method" (2.12) is

$$\sigma_{ij} = -C_e\Delta \left\{ 2(e^r_{sgs})^{1/2}\, S_{ij} + \left(\frac{27}{8\pi}\right)^{1/3} C_s^{2/3}\Delta \left[C_1 \left(S_{ik}S_{kj} - \tfrac{1}{3}\, S_{mn}S_{nm}\, \delta_{ij} \right) + C_2 \left(S_{ik}\, \Omega_{kj} - \Omega_{ik}\, S_{kj} \right) \right] \right\}. \tag{3.4}$$

Here the model parameter C_e is related to the Smagorinsky constant in the following way (Lilly 1967):

$$C_e = \pi^{1/3} \left(\frac{2}{3C_K} \right)^{1/2} C_s^{4/3} = \left(\frac{8\pi}{27} \right)^{1/3} C_s^{4/3}, \tag{3.5}$$

where C_K denotes the Kolmogorov constant for which we assumed the experimentally determined value $C_K \approx 1.5$. In a similar Reynolds stress model proposed by Pope (1975), the model parameters (transport coefficients) were determined as a function of both the turbulent kinetic energy and the dissipation rate.

The nonlinear model parameters C_1 and C_2 are determined so that the model provides correct energy transfer and captures the normal stress effects observed in homogeneous sheared flows.

4. Nonlinear SGS model parameters

Linear SGS models are characterized by only one model parameter, the Smagorinsky constant. The nonlinear SGS model presented in the previous section includes three model parameters. In addition to the Smagorinsky constant, for the nonlinear

model we have to determine the values of parameters associated with the second-order term in the strain rate tensor and the term related to the product of the strain rate tensor and the rotation rate tensor. However, we will show that these three parameters are not independent. The Smagorinsky constant as well as the parameter associated with the second-order term in the strain rate tensor will be determined by considering the inertial transfer of TKE. We will combine Lilly's (1967) approach to determining the Smagorinsky constant with that of Leslie & Quarini (1979) and Mason & Thomson (1992) for estimation of the energy backscatter.

To make the analytical procedure possible we adopt some common assumptions. We consider locally isotropic high-Reynolds-number turbulence in equilibrium. In this case the TKE production is balanced by dissipation. Furthermore we assume that due to the separation between the energy-producing scales of motion and dissipative scales the inertial subrange is developed and the energy spectrum follows Kolmogorov's $-5/3$ scaling law. We separate the large-scale from the small-scale component of the total flow field by defining the isotropic wave cut-off filter with the cut-off wavenumber k_c in the inertial subrange. Ideally the cut-off wavenumber will be sufficiently far from both maxima of the TKE dissipation and the TKE production. In statistical equilibrium the total dissipation of TKE by the small unresolved scales of motion is balanced by the influx of TKE due to the inertial transfer by the energy cascade mechanism

$$\langle \epsilon \rangle = T(k_c). \tag{4.1}$$

Here, ϵ is the the dissipation rate. In the spirit of Lilly's development, the ensemble average is approximated by the volume average corresponding to the smallest possible volume for which the statistical stability is still guaranteed. The input of TKE in the small-scale field due to the inertial transfer through the cut-off wavenumber k_c is denoted by $T(k_c)$ and defined as the integral of the inertial transfer spectrum (cf. McComb 1990, equation (2.119)) from the wavenumber zero to the cut-off wavenumber.

It should be pointed out that $T(k_c)$ also includes the local reverse flow of energy from small to large scales due to the interactions with the modes with wave-vector magnitude greater than the cut-off wave vector magnitude k_c. If the forward and backward components of the inertial transfer of energy are separated we can write

$$\langle \epsilon \rangle = T(k_c) = [C_f(k_c) - C_b(k_c)]\langle \epsilon \rangle \qquad \forall\ k_c \quad \text{in inertial range.} \tag{4.2}$$

Here, $C_f(k_c)$ is the coefficient of the forward scatter of energy while $C_b(k_c)$ denotes the backscatter. Both of these quantities are positive semi-definite and from (4.2) the forward scatter is always greater than the backscatter

$$C_f(k_c) - C_b(k_c) = 1 \qquad \forall\ k_c \quad \text{in inertial range.} \tag{4.3}$$

In LES the inertial transfer of energy $T(k_c)$ between resolved and subgrid scales is accounted for by the SGS term. When using an absolutely dissipative SGS model, the backscatter parameter is implicitly set to zero and consequently the forward-scatter parameter is set to one. However, the analysis of the nonlinear interactions in wave space as well as DNS results show that the backscatter parameter is non-zero. The consequence of setting $C_b = 0$ is that the model parameters can be uniquely determined by TKE balance considerations.

The backscatter parameter C_b was first defined by Leslie & Quarini (1979, equation (4.8)) and later used by Mason & Thomson (1992). Leslie & Quarini computed this parameter using eddy damped quasi-normal Markovian (EDQNM) statistical

turbulence theory and found that for the wave cut-off filter the value of this parameter varies between 1.4 and 0.4, depending on the shape of the TKE production spectra. For the input of TKE at the zeroth mode, only the highest value of 1.4 was obtained. Mason & Thomson (1992) used this value in their backscatter model. Schumann (1995) determined the upper limit for the value of the backscatter parameter for his stochastic backscatter model at 0.43. Using the non-local EDQNM approximation he also found that $C_b = 0.176$ when the filter is smooth and only the largest scales experience backscatter. Domaradzki *et al.* (1993) computed the forward and backward scatter of energy from their DNS of a Taylor–Green vortex, and for different values of the cut-off wavenumber found that the ratio of the backscattered TKE to the forward-scattered TKE increases by increasing the cut-off wavenumber. When the backscatter parameter corresponding to their calculations is determined, it varies between 1.06 and 2.83 depending on the cut-off wavenumber. The higher value of the backscatter parameter corresponds to the higher cut-off wavenumber of 40 while the lower value corresponds to the cut-off wavenumber of 20. The DNS used for this analysis provided the maximum wave number of 170. The DNS was a low-Reynolds-number simulation and the inertial range was not developed. The dissipation rate peaked at wavenumber 20 which means that in both cases the cut-off wavenumber was in the dissipation range. We therefore conclude that by using DNS results we are not able to predict the behaviour of the backscatter parameter in high-Reynolds-number flows. However, if we compare DNS results to those obtained by EDQNM we can expect the backscatter parameter to decrease further when the cut-off wavenumber falls between the TKE spectrum peak and the dissipation rate peak. Therefore the lower value of the backscatter parameter seems more representative of the values that can be expected when the cut-off wavenumber is in the inertial range. Such reasoning is supported by the results of EDQNM theory calculations of Leslie & Quarini with a broad-band production spectra.

To determine the nonlinear model parameters we start with the SGS kinetic energy balance for the isotropic turbulence in equilibrium

$$\langle \epsilon \rangle = -\langle \sigma_{ij} S_{ij} \rangle. \tag{4.4}$$

Introducing the SGS stress model in (4.4), the following equation is obtained:

$$\langle \epsilon \rangle = (C_s \Delta)^2 \left\langle 2 \left((2 S_{mn} S_{mn})^{1/2} S_{ij} S_{ji} + C_1 S_{ik} S_{kj} S_{ji} \right) \right\rangle. \tag{4.5}$$

The second term on the right-hand side of (4.5) includes both isotropic and anisotropic components of the tensor $S_{ik}S_{kj}$, while our model given by equation (3.3) or (3.4) includes only its anisotropic component. The contribution of the isotropic component to the transfer of energy is identically zero since $\frac{1}{3}(S_{mn}S_{mn})\,\delta_{ij}\ S_{ij} \equiv 0 \quad \Rightarrow \left(S_{ik}S_{kj} - \frac{1}{3}\ S_{mn}S_{mn}\ \delta_{ij}\right) S_{ij} \equiv S_{ik}S_{kj}S_{ij}$. The component of the nonlinear SGS model involving the rotation rate tensor does not appear in the TKE energy balance (4.5) since a contraction of a symmetric by an antisymmetric tensor is identically zero, $S_{ik}\Omega_{kj}S_{ij} \equiv \Omega_{ik}S_{kj}S_{ij} \equiv 0$.

We will find relation between the model parameters – the Smagorinsky constant, C_s, and the nonlinear model parameter, C_1 – and the backscatter parameter C_b. Assuming isotropic turbulence, the contribution of the linear component of the SGS

model to the inertial transfer can be related to the velocity derivative (Lilly 1967; Tennekes & Lumley 1972)

$$\langle S_{ij}S_{ij}\rangle = \frac{30}{4}\left\langle \left(\frac{\partial u_1^r}{\partial x_1}\right)^2 \right\rangle. \tag{4.6}$$

The last term on the right-hand side of equation (4.5) can be related to the determinant of the strain rate tensor, which can in a general three-dimensional flow be either positive or negative, unlike the second invariant $S_{ij}S_{ij}$ which is positive semi-definite for any flow except uniform-velocity laminar flows, when it vanishes. It is important to notice that in the case of two-dimensional flow the nonlinear term's contribution to the energy balance vanishes since in that case $\det(S_{ij}) = 0$. In the case of isotropic turbulence the third invariant can be directly related to the enstrophy production by the vortex stretching. For flows with non-zero enstrophy production the determinant of the strain rate tensor is always negative. Expanding the determinant of the strain rate tensor and using the isotropic form of a general sixth-order tensor (see the Appendix in Champagne 1978) it is easy to show that

$$\langle S_{ik}S_{kj}S_{ij}\rangle = \frac{105}{8}\left\langle \left(\frac{\partial u_1^r}{\partial x_1}\right)^3 \right\rangle = \frac{3}{4}\omega_i^r\omega_j^r\frac{\partial u_i^r}{\partial x_j}. \tag{4.7}$$

From (4.7) it follows that in the case of enstrophy production characterized by a negative term on the far right-hand side, the third invariant of the strain rate tensor is negative.

By analogy to the skewness factor (cf. Bachelor 1953) we define a skewness function $\mathscr{S}(k_c)$ as a skewness factor of the resolved velocity field, as such a function of the wave cut-off number

$$\mathscr{S}(k_c) = -\left\langle \left(\frac{\partial u_1^r}{\partial x_1}\right)^3 \right\rangle \Big/ \left\langle \left(\frac{\partial u_1^r}{\partial x_1}\right)^2 \right\rangle^{3/2}. \tag{4.8}$$

Notice that when $k_c \to \infty$ then $\mathscr{S}(k_c) \equiv s$, where s is the skewness factor. Now we can relate the linear and the nonlinear SGS contribution to the inertial transfer of energy as well as to each other. Introducing the skewness function is justified by the fact that it enables us to relate the third to the second moment of the resolved velocity derivative and thus simplify the modelling procedure. The skewness function, $\mathscr{S}(k_c)$, of a resolved velocity field in isotropic turbulence is a measurable quantity. It is a function of the cut-off wavenumber only. Enstrophy production peaks in the inertial range and therefore we can expect that with the cut-off wavenumber in the inertial subrange, the skewness function $\mathscr{S}(k_c)$ assumes a value comparable to that of the skewness factor s based on the total field. In low-Reynolds-number laboratory experiments the skewness factor is estimated to be 0.4 (Bachelor 1953) while experiments in the atmosphere give the value of 0.8 (Wyngaard & Tennekes 1970; Champagne 1978). Wyngaard & Tennekes (1970) argued that the skewness factor is Reynolds-number dependent.

The physical significance of the skewness factor is that it can be viewed as a non-dimensional measure of the rate of enstrophy production by vortex stretching induced by shear (Bachelor & Townsend 1947). It is obvious that to produce enstrophy by vortex stretching, the skewness factor must be positive. Vortex stretching is a mechanism underlying the cascade of energy and therefore the implicit inclusion of the skewness factor in the nonlinear model can be viewed as a desirable feature of any SGS parameterization.

The velocity derivative correlation in the denominator of the expression for the skewness function (4.8) can be determined in relation to the energy spectrum. The velocity-gradient correlation tensor for isotropic turbulence can be related to the energy spectrum (Bachelor 1953) so that

$$\left\langle \frac{\partial u_i^r}{\partial x_j} \frac{\partial u_m^r}{\partial x_n} \right\rangle = \int\limits_{\substack{\boldsymbol{k} \\ k \leqslant k_c}} k_j k_n \, \frac{E(k)}{2\pi k^2} \, (-k_i k_m + \delta_{im} k^2) \, \mathrm{d}\boldsymbol{k}. \tag{4.9}$$

Here, $E(k)$ is the spectrum shape for the isotropic turbulence. For the second equality we used the general isotropic form of the energy spectral density and assumed reflectional symmetry. Now, we invoke Kolmogorov's (1941) scaling law in the wavenumber form

$$E(k) = C_K \, \langle \epsilon \rangle^{2/3} \, k^{-5/3}. \tag{4.10}$$

Using the spectrum shape (4.10), setting indices i, j, m, n in equation (4.9) equal to 1, and integrating over spherical shells defined by $k = \text{const}$, the following expression is obtained:

$$\left\langle \left(\frac{\partial u_1^r}{\partial x_1} \right)^2 \right\rangle = \tfrac{1}{10} C_K \, \langle \epsilon \rangle^{2/3} \, k_c^{4/3}. \tag{4.11}$$

Using the expression for the skewness function and (4.11), the third and the second moments of the velocity derivative can be related to the resolved strain rate tensor magnitude:

$$\left\langle \left(\frac{\partial u_1^r}{\partial x_1} \right)^3 \right\rangle = -\mathscr{S}(k_c) \left\langle \left(\frac{\partial u_1^r}{\partial x_1} \right)^2 \right\rangle^{3/2} = -\mathscr{S}(k_c) \, \left(\tfrac{1}{10} C_K \right)^{3/2} \, \langle \epsilon \rangle \, k_c^2. \tag{4.12}$$

Introducing these equalities into (4.5) and assuming that $\langle (S_{mn} S_{mn})^{1/2} S_{ij} S_{ij} \rangle \approx \langle S_{kl} S_{kl} \rangle^{3/2}$ when the ensemble average is approximated by the grid volume average (Lilly 1966) results in the following expression for the ensemble-averaged dissipation rate:

$$\langle \epsilon \rangle = (C_s \Delta)^2 \left[1 - \frac{7}{960^{1/2}} \, C_1 \, \mathscr{S}(k_c) \right] \left(\tfrac{3}{2} C_K \right)^{3/2} \, k_c^2 \, \langle \epsilon \rangle. \tag{4.13}$$

The cut-off wavenumber can be related to the grid size Δ so that $k_c = \pi/\Delta$. After dividing through (4.13) by the ensemble-averaged dissipation rate and introducing an expression for the cut-off wavenumber k_c as well as the experimentally determined value for the Kolmogorov constant $C_K \approx 1.5 = 3/2$, we can express the model parameters as functions of the backscatter parameter and the skewness function:

$$C_s = \left[\frac{8 \, (1 + C_b)}{27 \, \pi^2} \right]^{1/2}. \tag{4.14}$$

Similarly the nonlinear model parameter C_1 is

$$C_1 = \frac{960^{1/2} \, C_b}{7 \, (1 + C_b) \, \mathscr{S}(k_c)}. \tag{4.15}$$

Only the nonlinear term parameter C_1 depends on both the backscatter parameter and the skewness function. The backscatter parameter is positive semi-definite. Owing to the prevalence of the enstrophy production by vortex stretching compared to the enstrophy destruction, the skewness function is almost always positive when the corresponding cut-off wavenumber is in the inertial range. It follows that the nonlinear model parameter C_1 will almost always be positive. Consequently the ensemble-mean

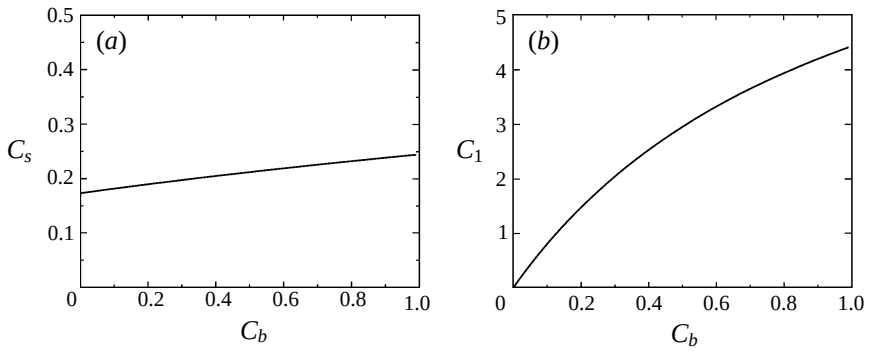

FIGURE 1. Model parameters: (*a*) Smagorinsky constant, (*b*) nonlinear model parameter.

contribution of the nonlinear term to the energy balance is either negative or it vanishes. In contrast to the linear SGS term which on average contributes to the forward cascade of energy, the nonlinear term on average contributes to the backscatter of energy. We are not aware of any direct way to determine the backscatter parameter based on any of the fundamental principles even in the most simple case of isotropic turbulence. We will therefore use the backscatter parameter as the fundamental model parameter, assuming that it is relatively insensitive to the cut-off wavenumber as long as the cut-off wavenumber is in the inertial range. However, we can expect it to depend on the level of anisotropy of the flow field. The Smagorinsky constant and the nonlinear model parameter C_1 as functions of the backscatter parameter are shown in figure 1. It is obvious that for a given range, the Smagorinsky constant is only a weak function of the backscatter parameter, unlike the nonlinear model parameter.

This analysis was based on the assumption that the resolved velocity field is isotropic. In most applications of interest this is not the case and therefore the results of our analysis represent the limiting case which our model has to satisfy. We expect the backscatter parameter in anisotropic flows to differ from the values obtained under the assumption of isotropy. The actual value of the backscatter parameter will be determined by a numerical experiment.

We have seen that the second model parameter C_2 cannot be determined from the TKE considerations, since the terms involving the rotation rate tensors do not contribute to the TKE balance. Therefore we have to consider their effects on the SGS stresses. There is a large body of experimental evidence that the anisotropic component of the turbulent stress in sheared turbulence displays notable differences in its normal stress components (Rose 1966; Tavoularis & Corrsin 1981; Rogers & Moin 1987) – these are so-called normal stress effects similar to those characteristic for non-Newtonian fluids. In order to extend those ideas to modelling SGS stresses, we adopt a simplified picture according to which the turbulent SGS flow field is locally subjected to the resolved shear in the same way that mean simple shear affects the homogeneous turbulent flow field. This will allow us to use the measured values of normal turbulent stresses in homogeneous turbulence subjected to the simple shear to determine the second nonlinear model parameter C_2.

We use the values of the normal turbulent stress components measured by Rose (1966). The isotropic component of the turbulent stress is subtracted and the following

values for the diagonal components of the anisotropic turbulent stress normalized by the TKE (denoted by $b_{\alpha\alpha}$) are obtained:

$$b_{11} \approx 0.11\dot{6} = \frac{35}{300}; \qquad b_{22} \approx -0.0\dot{3} = -\frac{10}{300}; \qquad b_{33} \approx -0.08\dot{3} = -\frac{25}{300}. \quad (4.16)$$

In more recent measurements Tavoularis & Corrsin (1981) and De Souza, Nguyen & Tavoularis (1995) obtained slightly higher absolute values of the diagonal components of the anisotropic turbulent stress. However, we use only the ratios of these components to determine the model parameters and these ratios are approximately the same in all the measurements.

In the case of simple shear the resolved strain rate tensor S_{ij} and the corresponding rotation rate tensor Ω_{ij} are

$$S_{ij} = \frac{1}{2}\frac{\mathrm{d}u_1^r}{\mathrm{d}x_3}\begin{pmatrix} 0 & 0 & 1 \\ 0 & 0 & 0 \\ 1 & 0 & 0 \end{pmatrix}; \qquad \Omega_{ij} = \frac{1}{2}\frac{\mathrm{d}u_1^r}{\mathrm{d}x_3}\begin{pmatrix} 0 & 0 & 1 \\ 0 & 0 & 0 \\ -1 & 0 & 0 \end{pmatrix}. \quad (4.17)$$

After introducing the strain rate and the rotation rate tensors corresponding to the simple shear into the nonlinear model (3.4) and requiring that the ratios of modelled normal stress components be the same as the ratios of measured stress components (4.16) it follows that the model parameters C_1 and C_2 must be approximately equal:

$$C_2 \approx C_1. \quad (4.18)$$

If the anisotropic normal stress components are defined exactly as the fractions in equation (4.16) then $C_2 = C_1$. Although we resorted to a heuristic argument and used the measured ratios of normal turbulent stresses to determine the model parameters for the SGS stresses, we can argue that such an approach is justified in the presence of the strong mean shear characteristic of surface layers of atmospheric boundary layers. Finally we conclude that the proposed nonlinear model along with the Smagorinsky constant can be characterized by only one additional parameter – the backscatter parameter, C_b. The backscatter parameter is the only free parameter that remains to be determined in the nonlinear SGS model. Lacking a theoretical basis we combine the empirical results obtained using DNS and EDQNM analysis with numerical experiments to determine the optimal value for the backscatter parameter. The results of this procedure are presented in the following section.

5. LES of a shear-driven atmospheric boundary layer

To test the nonlinear SGS model we perform an LES of a neutral shear-driven atmospheric boundary layer. We compare the results obtained using the linear model defined by (2.9) to those obtained by using the nonlinear SGS models defined by (3.4). In both cases an additional equation (2.13) for the evolution of SGS kinetic energy was integrated along with the resolved momentum equation (2.1). The eddy viscosity for the linear model was determined using (2.12). The resolved field equations were spatially discretized using the algorithm developed by Moeng (1984), with pseudo-spectral decomposition for horizontal homogeneous directions and central differences for the vertical. Instead of the Adams–Bashforth scheme used by Moeng (1984) we used the fourth-order Runge–Kutta scheme to integrate the equations in time. The approximate boundary condition based on the Monin–Obukhov similarity relationship (Moeng 1984) was implemented at the surface while the stress-free boundary condition was imposed at the upper free-flow boundary.

The flow was driven by the mean pressure gradient corresponding to a 10 m s^{-1} geostrophic wind in the stream-wise direction with no cross-stream component at 45° North. The surface roughness length was 0.1 m. The resulting time-averaged surface friction velocity u_* was approximately 0.48 m s^{-1}. The computational domain was 4000 m × 2000 m × 1500 m, discretized by 40^3 and 60^3 grid points distributed uniformly in each direction. The domain size, initial conditions and the domain resolution were the same as in Andrén *et al.* (1994), so that our results could be compared to those obtained from three different LES codes (Schumann 1975; Moeng 1984; Mason & Thomson 1987) which were presented by Andrén *et al.* (1994).

The nonlinear model parameters are determined by first choosing the appropriate backscatter parameter. The backscatter parameter can be determined using the DNS analysis or EDQNM calculations. Since the backscatter parameter is greater than zero the Smagorinsky constant will always attain a value greater than that estimated by Lilly (1967). Lilly's values for the Smagorinsky constant for different filters can be viewed as lower limits when $C_b = 0$. This may seem to be in contradiction to the results of numerical simulations which suggest that Lilly's value for the Smagorinsky constant is too large, yielding an SGS model that is too dissipative. However, those models could not account for the backscatter of energy. We started by assuming the value of the skewness function as $S(k_c) = 0.5$ and choosing the backscatter parameter $C_b = 0.4$ that corresponds to the wide-band production spectra in EDQNM of Leslie & Quarini (1979). This value of the backscatter parameter appeared to be too high, yielding an incorrect mean velocity profile. To determine the optimal value of the backscatter parameter we conducted a numerical experiment. We carried out five LES of shear-driven boundary layers and varied only the value of the backscatter parameter. In the first simulation we set $C_b = 0.4$ and then decreased it by 0.02 in consecutive simulations. Finally we conducted an LES with $C_b = 0.3$. We observed the effects of varying the backscatter parameter on the global statistics of the turbulent flow field, focusing our attention primarily on the mean velocity profiles. The numerical experiment showed that the optimal value of the backscatter parameter is $C_b = 0.36$. Because (4.14) and (4.15) are based on the isotropy assumption, the backscatter parameter value obtained using the numerical experiment does not imply that exactly 36% of dissipated energy is actually backscattered. The model parameters C_e and C_1 are then determined using (4.14), (3.5) and (4.15).

All simulation runs were ten hours or $3.6f^{-1}$ in non-dimensional time units. The results presented here represent ensemble averages over 300 data sets stored every minute during the last five hours ($1.8f^{-1}$) of the simulation runs. The iteration history of the resolved TKE as a function of time is shown in figure 2. The spin-up time for the nonlinear model is much shorter due to the backscatter effects. A fraction of the kinetic energy initially residing at small unresolved scales of motion is transferred to the large scales of motion through the nonlinear component of the SGS term. The nonlinear model results in much smaller TKE fluctuations than the linear model and therefore can be viewed as providing a more stable simulation.

Earlier we pointed out that the efficiency of the SGS model should be judged according to how well the LES reproduces the global statistics of the flow field. In the shear-driven atmospheric boundary layer (ABL) case the theoretical prediction for the mean velocity profile has been confirmed by the experiment. According to the Monin–Obukhov theory the mean wind shear in the surface layer of the shear-driven ABL is a function of the surface stress u_*, and the distance from the surface z, with

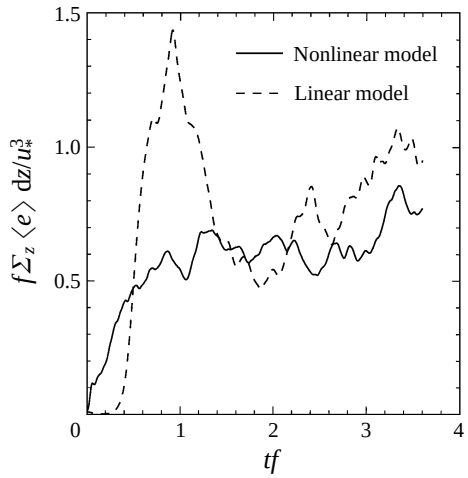

FIGURE 2. Time series of normalized total TKE.

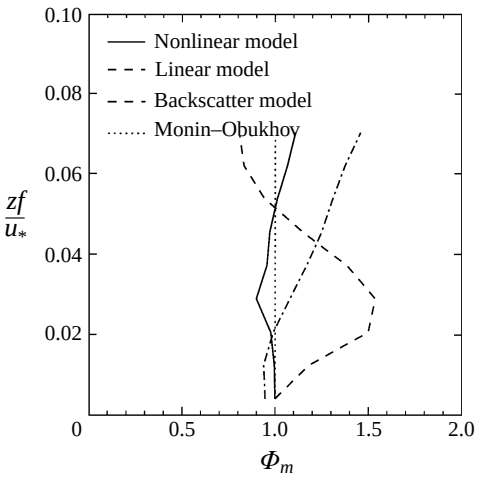

FIGURE 3. Non-dimensional shear (40^3 grid points), $\Phi_m = u_*/(\kappa z)$.

a constant of proportionality $1/\kappa$ where κ is von Kármán's constant. It follows that the non-dimensional shear Φ_m is unity:

$$\frac{\partial U}{\partial z} = \frac{u_*}{\kappa z} \quad \Rightarrow \quad \Phi_m = \frac{\kappa z}{u_*}\frac{\partial U}{\partial z} = 1. \tag{5.1}$$

Monin–Obukhov theory has been experimentally confirmed in a number of field experiments starting with the Kansas experiment (Businger *et al.* 1971) and represents one of the most firmly established results against which LES and new SGS models should be compared. The non-dimensional shear Φ_m is shown in figure 3. In addition to the results obtained using our LES algorithm with the linear and the nonlinear SGS model we plot the results of Andrén *et al.* obtained using the stochastic-backscatter model. The mean wind shear differs significantly between these models. While the non-dimensional shear obtained using the linear model exhibits the characteristic overshoot observed by Mason & Thomson (1992) as well as Sullivan *et al.* (1994), the nonlinear model with the backscatter parameter $C_b = 0.36$ follows closely the

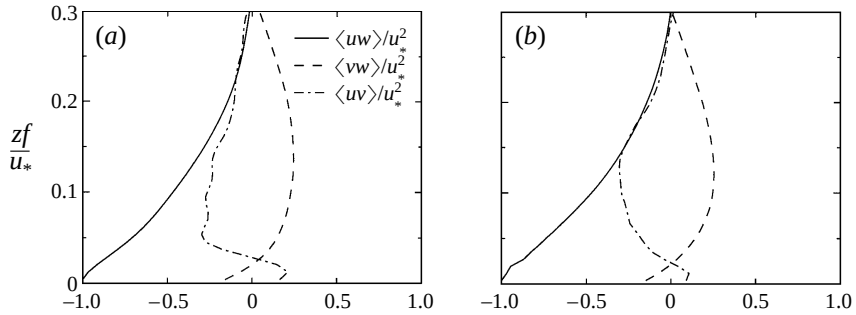

FIGURE 4. Tangential turbulent stresses: (*a*) linear SGS model, (*b*) nonlinear SGS model.

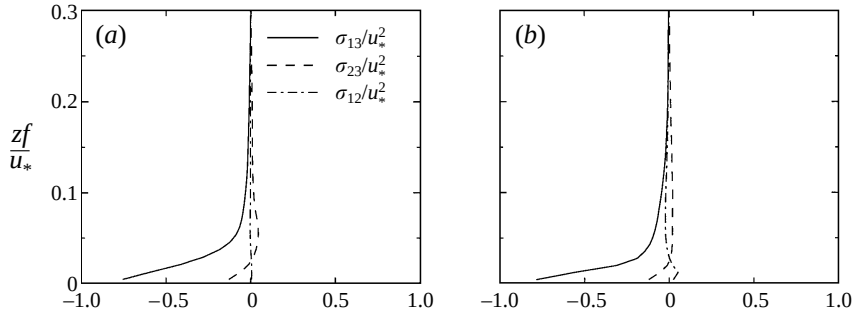

FIGURE 5. Tangential SGS stress components: (*a*) linear SGS model, (*b*) nonlinear SGS model.

predictions of the Monin–Obukhov theory and experimental results. In accordance with theory it results in a vanishingly small first derivative of the non-dimensional shear at the surface. We point out that when using the nonlinear model with $C_b > 0.36$ the non-dimensional shear in the surface layer was underestimated ($\Phi_m < 1$) while for $C_b < 0.36$ the non-dimensional shear was overestimated ($\Phi_m > 1$).

The reasons for the improvement in prediction of the mean shear can be detected by analysing the resolved and SGS TKE, corresponding turbulent stresses and the TKE budgets. The profiles of the total (resolved + subgrid) tangential turbulent stresses are show in figure 4. Both linear and nonlinear model simulations result in a full almost linear profile of the $\langle uw\rangle$ stress component, as predicted by theory. While the tangential stress component $\langle vw\rangle$ is almost identical in both simulations, the difference between simulations with the linear and nonlinear models is pronounced in the profiles of the $\langle uv\rangle$ stress component in the layer adjacent to the surface layer. However, the general trends are approximately the same and the more accurate profile of the stress component $\langle uv\rangle$ obtained using the nonlinear SGS model may be attributed to the more accurate prediction of the mean shear. It is interesting to notice that the tangential SGS stresses (figure 5) do not exhibit any significant differences between the two simulations. This was expected since the nonlinear model was designed to reproduce the normal stress effects and not to affect the tangential stresses.

To examine how the nonlinear model affects normal stresses we first plot the profile of the total TKE (figure 6). We observe that when the nonlinear model is used the TKE profile is almost linear, unlike the corresponding profile obtained with the linear model. In addition the TKE level in the surface layer is 30% lower for the nonlinear

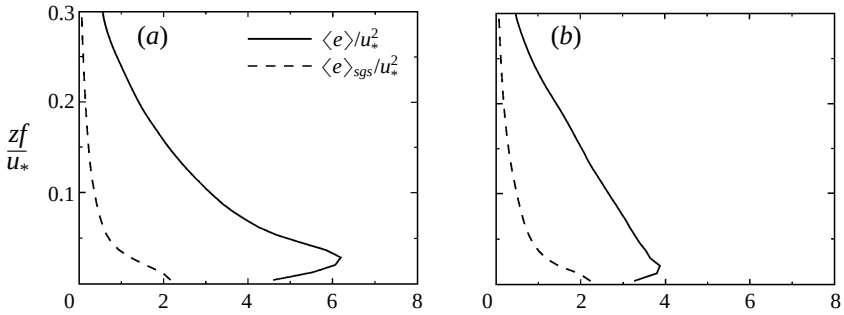

FIGURE 6. Total and subgrid TKE profiles: (*a*) linear SGS model, (*b*) nonlinear SGS model.

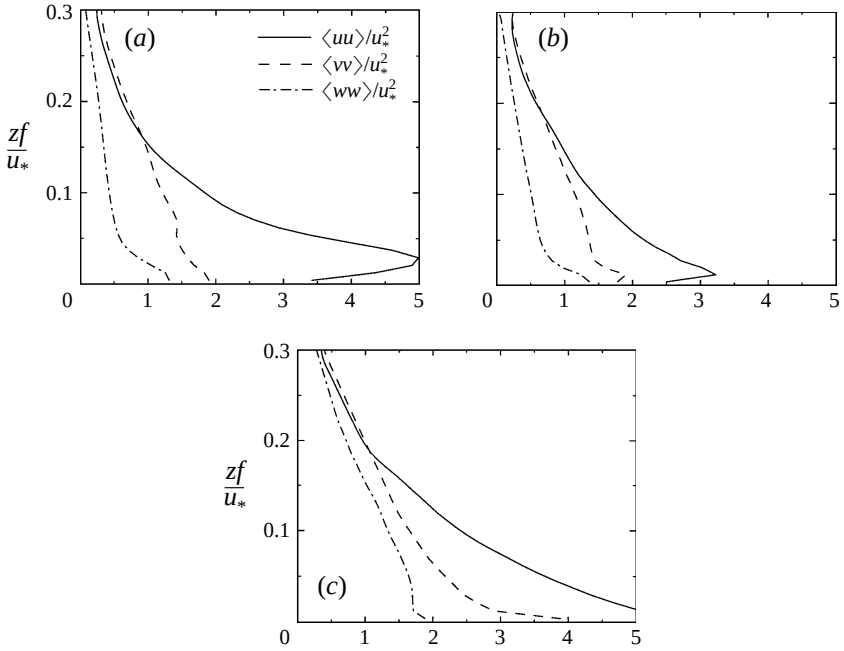

FIGURE 7. Normal stress components: (*a*) linear SGS model, (*b*) nonlinear SGS model, (*c*) stochastic backscatter model (results from Andrén *et al.* 1994).

model simulation. We examine these features more closely by comparing the total normal turbulent stress components (figure 7) and notice two major differences. When the nonlinear model is used the maximum of the streamwise normal stress component is 30% less than when the linear model is used and is essentially a linear function of the distance from the surface. The vertical normal stress component is almost identical in both simulations. In addition we plot normal stresses obtained using the stochastic-backscatter model by Andrén *et al.* (1994) (figure 7*c*). The backscatter model results in all three normal stress components near the surface being larger than when the other two models are used. The shape of the profiles and the relative magnitudes of the components are similar to those obtained using the linear model. All observed differences are solely the consequence of the differences in the SGS models. We developed the nonlinear SGS model to account for the effects of anisotropy due to the shear. The effects of shear and the associated intrinsic vorticity are manifested

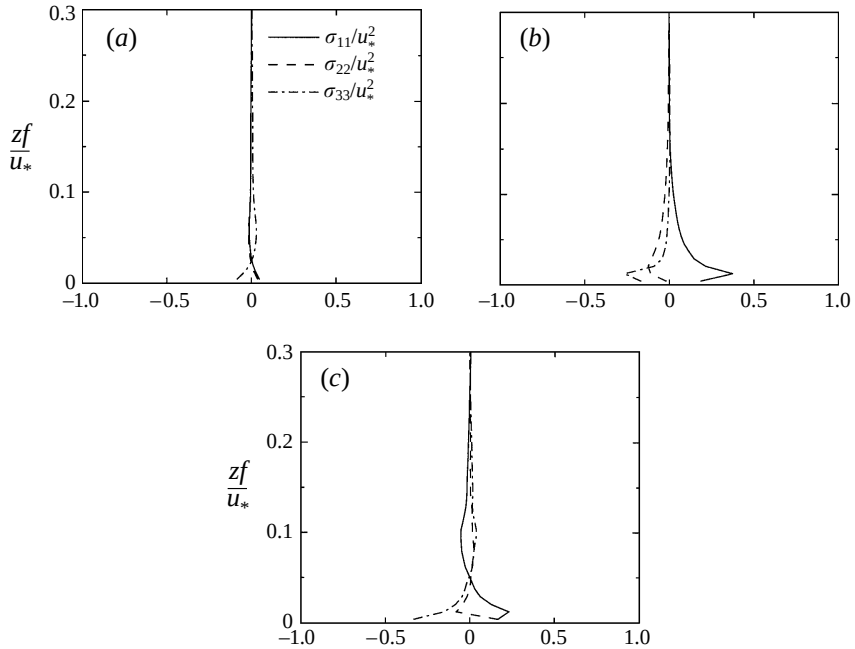

FIGURE 8. Anisotropic normal SGS stress components: (*a*) linear SGS model, (*b*) nonlinear SGS model, (*c*) stochastic backscatter model (results from Andrén *et al.* 1994).

as Coriolis effects that are responsible for increased anisotropy levels among normal SGS stress components. We can therefore expect that the observed differences are the consequence of the differences among the normal components of the SGS stresses. The profiles of the anisotropic normal SGS stress components reveal (figure 8) that the linear model is not capable of reproducing the normal stress effects. While the linear model results in almost vanishing anisotropic normal stress components, the nonlinear model produces a streamwise component with near the surface maximum of almost 50% of the surface stress. At the same time the cross-stream and vertical components are non-zero and exhibit a more complex behaviour as a function of the distance from the surface. From the results of Andrén *et al.* we computed the anisotropic components of normal subgrid stresses obtained using the backscatter model. These profiles are shown in figure 8(*c*) and we notice that near the surface they are similar to those obtained using the nonlinear model while above the surface layer they exhibit the sign change.

The TKE budgets shown in figure 9 reveal that the nonlinear model results in a significant reduction of the TKE transport. In the same time a most important difference can be observed in the dissipation rate profile or more precisely in the rate of inertial transfer of energy toward the unresolved scales of motion. When the linear SGS model is used the inertial transfer peaks at the surface while the nonlinear model causes an elevated maximum at some height above the surface corresponding to the level of maximum TKE production. This may seem to contradict the usually accepted picture whereby the inertial transfer toward unresolved scales peaks at the surface. While it is obvious that the actual dissipation rate caused by the viscous effects must have a maximum at the surface, the inertial transfer in LES does not have to behave in the same way. Since in the surface layer the TKE production mechanism is not completely resolved we can expect an increased energy backscatter level in that

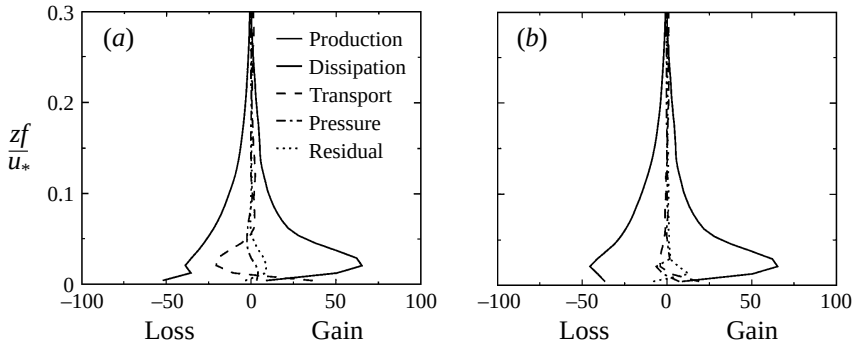

FIGURE 9. Normalized TKE budget: (*a*) linear SGS model, (*b*) nonlinear SGS model.

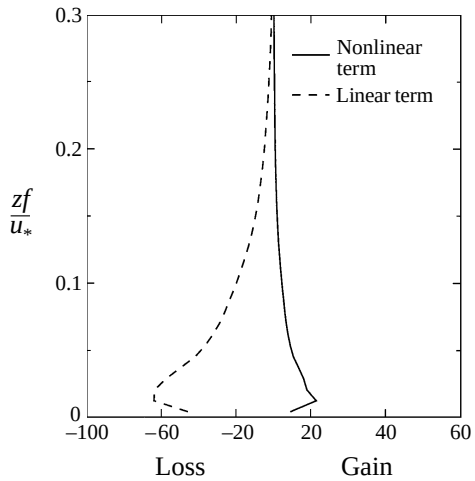

FIGURE 10. Linear and nonlinear term contributions to the rate of inertial transfer of TKE (dissipation and backscatter).

region. This backscattered energy will in turn cause an apparent reduction of the inertial transfer rate. Whether this actually happens when a nonlinear model is used can be observed by separating the inertial transfer due to the linear component of the nonlinear SGS model from the contribution of the nonlinear component. Figure 10 clearly shows that such an elevated inertial transfer rate maximum is indeed caused by the backscatter which balances the forward cascade of TKE at the levels adjacent to the surface.

We examine the boundary layer structures using two-dimensional correlation functions. In figure 11 we compare the streamwise velocity correlation functions obtained using the linear and nonlinear SGS models. Although the streamwise velocity does not decorrelate itself in the given domain, a feature commonly observed not only in computations (Mason & Thomson 1987) but also in the laboratory experiments, a striking difference in the size of the structures associated with the higher correlation values (greater than 0.2) can be observed near the surface ($zf/u_* = 0.05$). No such difference is observed at $zf/u_* = 0.2$ (figure 12) or in the cross-stream velocity correlation at any level (figure 13 and figure 14). However, the vertical velocity correlation function displays features similar to the streamwise one. While the linear SGS model

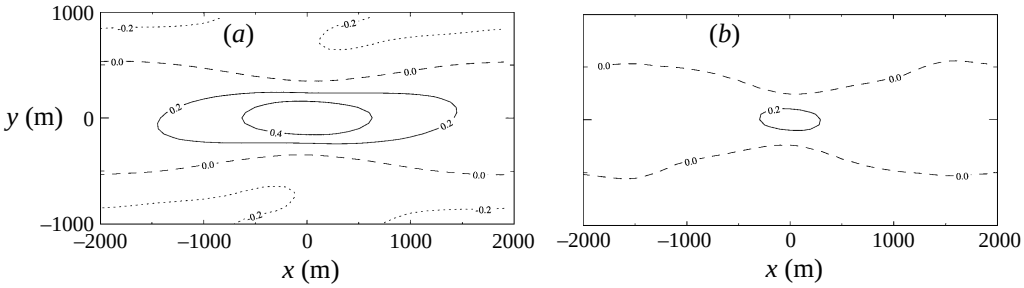

FIGURE 11. Streamwise velocity correlation function at $zf/u_* = 0.05$: (*a*) linear SGS model, (*b*) nonlinear SGS model.

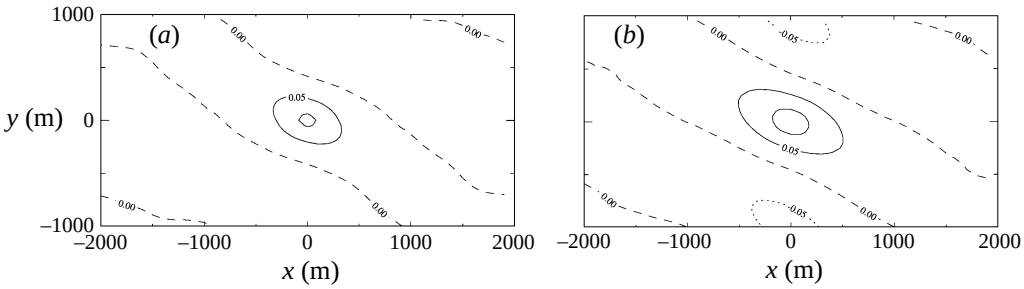

FIGURE 12. Streamwise velocity correlation function at $zf/u_* = 0.2$: (*a*) linear SGS model, (*b*) nonlinear SGS model.

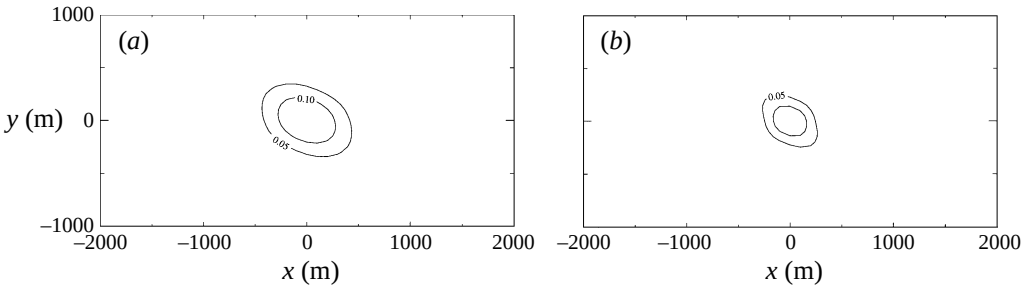

FIGURE 13. Cross-stream velocity correlation function at $zf/u_* = 0.05$: (*a*) linear SGS model, (*b*) nonlinear SGS model.

results in elongated structures near the surface, the nonlinear model produces smaller more isotropic structures (figure 15). Away from the surface both models produce similar vertical velocity structures (figure 16).

We performed a higher-resolution simulation with 60^3 grid points to test the nonlinear model for resolution dependence and to analyse characteristic flow structures in more detail. The non-dimensional shear for the same initial and boundary conditions representing the average over the same time period, but for the increased resolution, is given in figure 17. It is obvious that the increased resolution result is in good agreement with theory and does not differ significantly from those obtained with lower resolution. We compare the streamwise velocity structures in horizontal planes in the surface layer obtained using the linear and nonlinear models (figure 18). The linear model simulation exhibits streaky streamwise velocity structures aligned with the mean wind. Such slow and fast streaks were also observed by Mason &

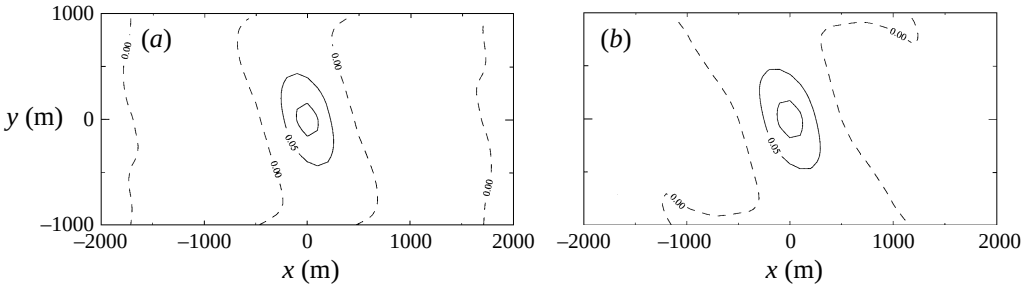

FIGURE 14. Cross-stream velocity correlation function at $zf/u_* = 0.2$: (*a*) linear SGS model, (*b*) nonlinear SGS model.

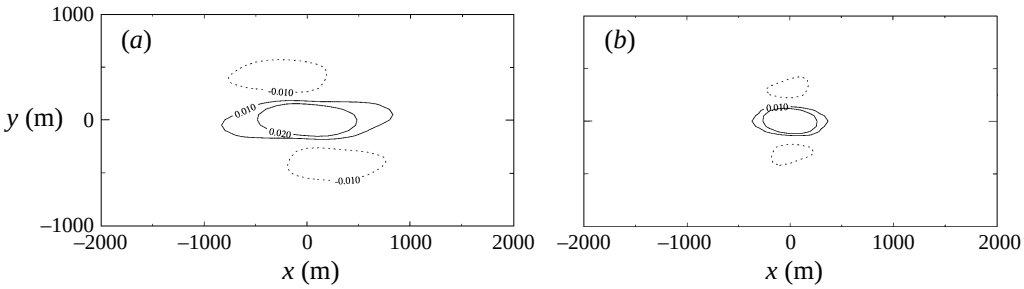

FIGURE 15. Vertical velocity correlation function at $zf/u_* = 0.05$: (*a*) linear SGS model, (*b*) nonlinear SGS model.

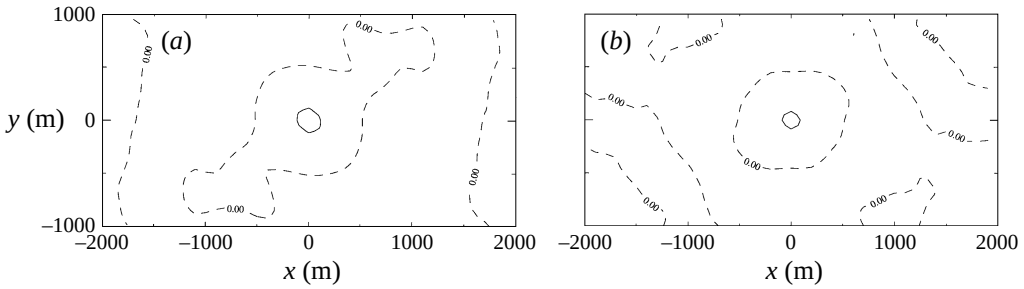

FIGURE 16. Vertical velocity correlation function at $zf/u_* = 0.2$: (*a*) linear SGS model, (*b*) nonlinear SGS model.

Thomson (1987) and Moeng & Sullivan (1994) in their simulations which utilised linear SGS models. In comparison, the LES with the nonlinear SGS model exhibits strikingly different flow structures. Although we can observe some poorly defined narrow and elongated fast streaks they are not aligned with the mean velocity vector and it is difficult to confirm their coherence. The one-dimensional streamwise spectra of three velocity components computed at three levels above the surface, $zf/u_* = 0.02, 0.05, 0.1$, are presented in figures 19–21. The spectra are averaged in time over the last five hours of the simulation and in space over the cross-steam flow direction. These spectra illustrate further the difference between simulations with the linear and the nonlinear SGS model. When the linear SGS model is used the spectra of all three velocity components corresponding to the lowest level $zf/u_* = 0.02$ drop off steeply with increasing wavenumber, indicating the dominance of larger structures. This confirms earlier observations based on the contour plots of the streamwise

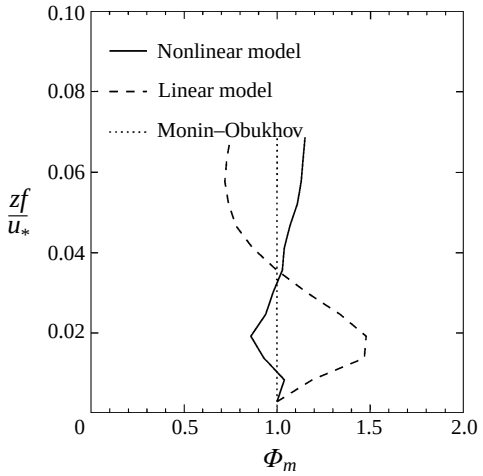

FIGURE 17. Non-dimensional shear (60^3 grid points), $\Phi_m = u_*/(\kappa z)$.

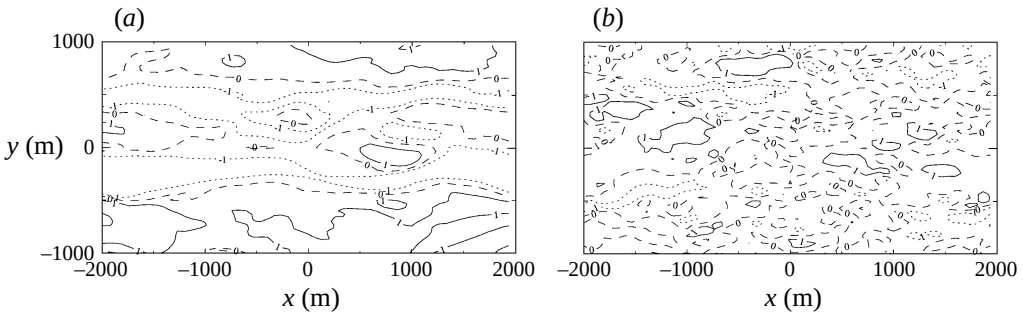

FIGURE 18. Streamwise velocity contours at $zf/u_* = 0.05$: (*a*) linear SGS model, (*b*) nonlinear SGS model. Solid line - positive fluctuating velocity, dashed line - horizontal mean velocity, dotted line - negative fluctuating velocity.

velocity as well as two-dimensional correlation functions. The simulation with the nonlinear SGS model produces spectra without such a steep drop-off and the spectral peak is shifted toward larger wavenumbers corresponding to smaller scales of motion. As a reference we plot on figures 19–21 the inertial-range $k^{-2/3}$ line. Although the resolution of the simulation is not sufficient to observe an extended inertial range the nonlinear SGS model results in a closer fit to the inertial range spectra than the linear SGS model.

In order to determine the values of nonlinear model parameters we assumed the experimental value of the skewness factor $\mathscr{S}(k_c) = 0.5$. The skewness factor as defined by equation (4.8) represents an unambiguous measure of vortex stretching only in the isotropic case. However, we can define the ratio of the third and the second invariants for the strain rate tensor multiplied by a factor of $(9/8)^{1/2}$ as a generalized skewness function, $\mathscr{S}_g(k_c)$, which in the isotropic case reduces to the skewness function $\mathscr{S}(k_c)$:

$$\mathscr{S}_g(k_c) = -\frac{\langle S_{mr}S_{rn}S_{nm}\rangle}{\langle S_{mn}S_{mn}\rangle^{3/2}} = \left(\frac{9}{8}\right)^{1/2} \frac{\langle III(S_{ij})\rangle}{\langle II(S_{ij})\rangle^{3/2}}. \tag{5.2}$$

The fact that the nonlinear model parameter is a function of the invariants of the

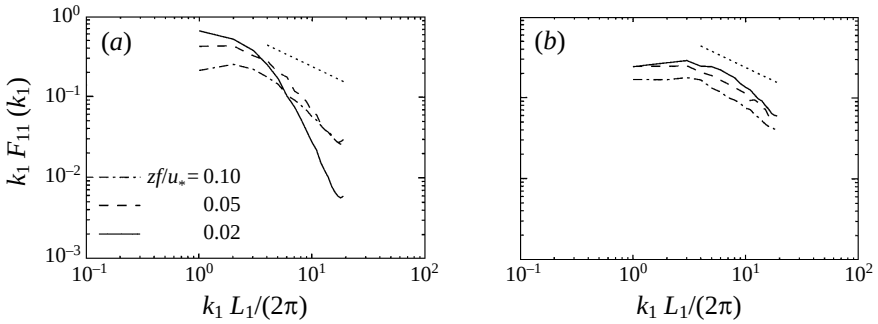

FIGURE 19. Streamwise velocity spectra at three levels above the surface ($zf/u_* = 0.02, 0.05, 0.1$): (*a*) linear SGS model, (*b*) nonlinear SGS model; the dotted line represents the inertial range $k^{-2/3}$ line.

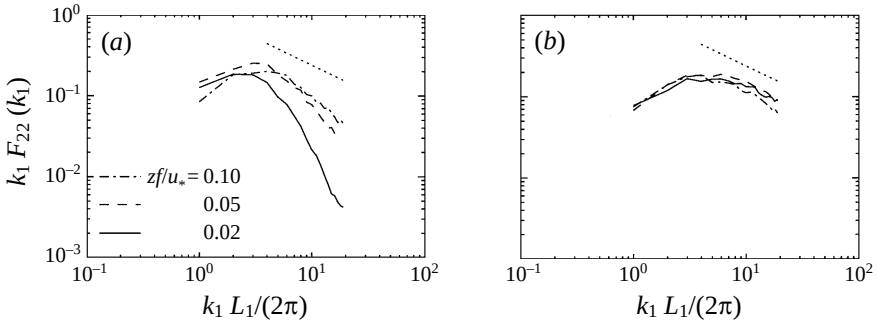

FIGURE 20. As figure 19 but for cross-stream velocity spectra.

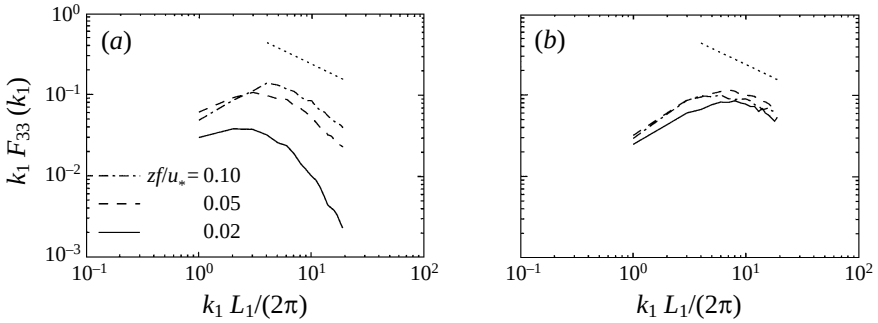

FIGURE 21. As figure 19 but for vertical velocity spectra.

strain rate tensor is consistent with the constitutive theory. The relation (5.2) can be viewed as a non-dimensional ratio of the ensemble average of the rate of inertial transfer of TKE to the corresponding TKE dissipation rate. The generalized skewness corresponding to the shear-driven ABL flow simulation is given in figure 22(*a*). The nonlinear model gives a somewhat higher value of the generalized skewness factor than the linear SGS model. The generalized skewness starts from the value of zero near the surface and then fast approaches a nearly constant value of slightly above 0.3. Using (4.6) and (4.7) we can compute the corresponding value of the skewness function of approximately 0.5 for the isotropic turbulence.

We determined the value of the backscatter parameter by numerical experiment and found that the optimal value of the parameter for the high-Reynolds-number

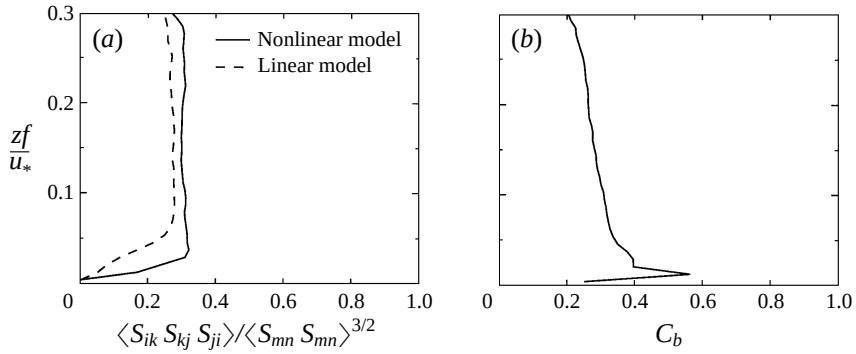

FIGURE 22. (*a*) Generalized skewness function, (*b*) backscatter parameter.

boundary layer simulation is $C_b = 0.36$. Since this value corresponds to the isotropic case and our ABL flow is neither isotropic nor homogeneous we can expect that the effective value of the backscatter parameter computed from the simulated flow field does not differ significantly from the estimated value. The effective backscatter parameter, C_{be}, can be determined from the following relation:

$$C_{be} = \frac{2(C_s\Delta)^2(2S_{mn}S_{mn})^{1/2}S_{ij}S_{ij} - \langle\epsilon\rangle}{\langle\epsilon\rangle}. \tag{5.3}$$

The dissipation rate $\langle\epsilon\rangle$ is computed using equation (4.1). The profile of the effective backscatter parameter (figure 22*b*) displays a sharp peak at the value of 0.55 near the surface and monotonically decreases with increasing distance from the surface, levelling off at the value of 0.2. The effective value of the backscatter parameter is close to the specified value $C_b = 0.36$ and to the value estimated using EDQNM theory for the broad-band production spectra. We can therefore conclude that the modelling problem for the nonlinear SGS model used in anisotropic and inhomogeneous turbulence LES can be reduced to determining the backscatter parameter for the isotropic turbulence which will give the desired value of the effective backscatter parameter in an actual (anisotropic and inhomogeneous) flow.

We point out that according to the Taylor–Proudman theorem (cf. Dutton 1995), flows in rotational frames characterized by a high Rossby number become two-dimensional, confined to the plane perpendicular to the axis of rotation. Since the skewness function vanishes in two-dimensional flows the nonlinear model parameter C_1 defined by (4.15) would exhibit singular behaviour for a finite value of the backscatter parameter. Moreover, as it was noted earlier, in the two-dimensional case the SGS stress model should be frame indifferent. A necessary and sufficient condition for frame indifference is that the nonlinear term, which includes the rotation rate tensor, vanishes. This can be accomplished by setting $C_2 = 2\mathscr{S}(k_c)C_1$ so that the nonlinear model parameter C_2 approaches zero in the limit of a two-dimensional flow. At the same time the parameter C_1 must be finite. The finiteness of C_1 is guaranteed if the lowest-order term in a power series expansion of the backscatter parameter in terms of the skewness function vanishes so that $C_b = a_1\mathscr{S}(k_c) + a_2[\mathscr{S}(k_c)]^2 + \ldots$. A backscatter parameter of this form results in a nonlinear model consistent with the frame indifference requirements in a two-dimensional flow limit. Determining the exact dependence of the backscatter parameter on the skewness function is a task that goes beyond the scope of this paper.

6. Discussion and conclusions

It has been recognized that the SGS model represents a limiting factor for the successful LES of high-Reynolds-number boundary layer flows. Two different approaches to solving the SGS problem have recently been proposed (Mason & Thomson 1992; Sullivan *et al.* 1994), both resulting in important improvements. However, questions about the true nature of the SGS problem in surface layers of the high-Reynolds-number boundary layers have remained open. Our goal was to focus on the critical element of the SGS model in order to develop a more consistent and efficient SGS model for such shear-driven flows.

We started our analysis of the SGS effects in the LES of high-Reynolds-number boundary layers by showing that only the fluctuating component of the SGS stress can affect the mean velocity profile. We showed that the SGS stress tensor is not frame indifferent and argued that the Coriolis effects caused by the intrinsic vorticity can increase the anisotropy level among the normal SGS stress components. Therefore we argued that the SGS models have to capture the effects of inertial transfer including backscatter of energy as well as its redistribution among the normal SGS stress components. The backscatter is the consequence of nonlinear interactions while the redistribution of SGS TKE is the consequence of anisotropy induced by shear.

To develop an SGS model able to reproduce the effects of anisotropy and that is easy to implement and computationally inexpensive, we adopted a phenomenological approach based on the nonlinear constitutive theory for viscous stresses. Models based on the nonlinear constitutive theory do not satisfy the second law of thermodynamics. They can result in a local backscatter of energy. At the same time they can account for the normal stress effects. We therefore developed a simple nonlinear extension to the classical Smagorinsky model and argued that it represents a viable choice for modelling SGS stresses. To determine the model parameters analytically, we analysed the isotropic case and the homogeneous shear flow case.

We implemented the nonlinear model in an LES of a shear-driven ABL and showed that unlike the linear model it yields the experimentally observed and theoretically predicted mean velocity profile. Furthermore application of the nonlinear model resulted in a significant redistribution of TKE among SGS normal stress components. The nature of the nonlinear model is such that it was impossible to isolate the cause and unambiguously determine whether its ability to reproduce the backscatter of energy or normal stress effects was crucial to achieve the observed improvements. Our analysis indicates that for the nonlinear model both of these characteristics were equally important. This confirms the basic premise that no adjustment of the linear model parameters (eddy viscosity, Smagorinsky constant) can result in improved LES of high-Reynolds-number boundary layers.

We explored the characteristic flow structures in the ABL by analysing the two-dimensional correlation function for the velocity components as well as instantaneous velocity fields. The analysis revealed that in comparison to the linear model (Sullivan *et al.* 1994), the nonlinear model significantly reduces the size of the streamwise velocity (slow and fast) streaks as well as the vertical velocity structures in the surface layer. Pronounced elongated streaks were also observed experimentally (Kim, Klein & Reynolds 1971) and in numerical simulations (Moin & Kim 1982) in viscous sublayers of moderate-Reynolds-number boundary layer flows. We therefore argue that their presence in the LES of an ABL can be attributed to the low-Reynolds-number effect induced by the linear SGS model.

The nonlinear SGS model developed and tested in this work is simple to implement and computationally inexpensive. It is also consistent with the constitutive theory

and satisfies basic requirements regarding the LES performance. We can therefore conclude that this nonlinear model represents a good alternative for LES of high-Reynolds-number boundary layer flows. Moreover we can expect this nonlinear model to improve LES of stably stratified ABLs as suggested by Canuto & Minotti (1993). These simulations have proven to be difficult due to the low level of TKE and intermittent nature of the flow. Nonlinear models of different levels of complexity are already extensively used in Reynolds stress closures for complex engineering flows. Applying similar modelling concepts to SGS modelling may prove to be a viable path toward efficient LES of complex engineering and geophysical flows.

This research was supported by a grant from NASA FIRE. The author would like to express his deepest gratitude to Dr Judith A. Curry for her valuable comments.

Appendix A. Material frame indifference and the SGS stress tensor

The group of transformations is given by

$$x_i^* = Q_{ij}(t)\, x_j + c_i(t). \tag{A 1}$$

Then, velocity fields $\tilde{u}_i$ transform under this group of transformations as

$$\tilde{u}_i^* = \dot{Q}_{ij}\, x_j + Q_{ij}\, \tilde{u}_j + \dot{c}_i. \tag{A 2}$$

Here, $\dot{c}_i$ denotes the time derivative of c_i and $\dot{Q}_{ij}$ denotes the time derivative of the orthogonal rotation tensor Q_{ij}. The resolved component of the transformed velocity field is defined as

$$\tilde{u}_i^{*r} = \int G^*(\boldsymbol{x}^* - \boldsymbol{\xi})\, \tilde{u}_i^*\, \mathrm{d}\boldsymbol{\xi}. \tag{A 3}$$

Ideally the filter function $G(\boldsymbol{x})$ is isotropic and it does not change under the transformation (A 1): $(G^*(\boldsymbol{x}) = G(\boldsymbol{x}))$. Also, since the transformation (A 1) is volume preserving it follows that $\mathrm{d}\boldsymbol{x}^* = \mathrm{d}\boldsymbol{x}$. Introducing equation (A 2) into (A 3) gives

$$\tilde{u}_i^{*r} = \int G(\boldsymbol{x} - \boldsymbol{\xi})\, [\dot{Q}_{ij}\xi_j + Q_{ij}\tilde{u}_j + \dot{c}_i]\, \mathrm{d}\boldsymbol{\xi}. \tag{A 4}$$

After integrating the right-hand side the resolved component of the transformed velocity is

$$\tilde{u}_i^{*r} = \dot{Q}_{ij}x_j + Q_{ij}\tilde{u}_j^r + \dot{c}_i. \tag{A 5}$$

The corresponding subgrid velocity component is defined as

$$\tilde{u}_i^{*s} = \tilde{u}_i^* - \tilde{u}_i^{*r}. \tag{A 6}$$

Then it follows that the subgrid velocity component transforms as

$$\tilde{u}_i^{*s} = Q_{ij}\tilde{u}_j^s. \tag{A 7}$$

The SGS stress is defined as

$$\tau_{ij} = (\tilde{u}_i^r\tilde{u}_j^r)^r - \tilde{u}_i^r\tilde{u}_j^r + \left[(\tilde{u}_i^r\tilde{u}_j^s + \tilde{u}_i^s\tilde{u}_j^r) + \tilde{u}_i^s\tilde{u}_j^s\right]^r. \tag{A 8}$$

Similarly the transformed SGS stress is

$$\tau_{ij}^* = (\tilde{u}_i^{*r}\tilde{u}_j^{*r})^r - \tilde{u}_i^{*r}\tilde{u}_j^{*r} + \left[(\tilde{u}_i^{*r}\tilde{u}_j^{*s} + \tilde{u}_i^{*s}\tilde{u}_j^{*r}) + \tilde{u}_i^{*s}\tilde{u}_j^{*s}\right]^r. \tag{A 9}$$

Any tensor T_{ij} that satisfies material frame indifference transforms as

$$T_{ij}^* = Q_{im}Q_{jn}T_{mn}. \tag{A 10}$$

The transformed SGS stress tensor can be obtained by rewriting equation (A 9) using (A 5) and (A 7):

$$\begin{aligned}\tau^*_{ij} = Q_{im}Q_{jn}\{&(\tilde{u}^r_m\tilde{u}^r_n)^r - \tilde{u}^r_m\tilde{u}^r_n + \left[\tilde{u}^r_m\tilde{u}^s_n + \tilde{u}^s_m\tilde{u}^r_n + \tilde{u}^s_m\tilde{u}^s_n\right]^r\}\\ &-Q_{im}\dot{c}_j\left[\tilde{u}^r_m - (\tilde{u}^r_m)^r - (\tilde{u}^s_m)^r\right] - Q_{jn}\dot{c}_i\left[\tilde{u}^r_n - (\tilde{u}^r_n)^r - (\tilde{u}^s_n)^r\right]\\ &-Q_{im}\dot{Q}_{jn}\left[x_n\tilde{u}^r_m - (\xi_n\tilde{u}_m)^r\right] - \dot{Q}_{im}Q_{jn}\left[x_m\tilde{u}^r_n - (\xi_m\tilde{u}_n)^r\right]\\ &-\dot{Q}_{im}\dot{Q}_{jn}\left[x_mx_n - (\xi_m\xi_n)^r\right].\end{aligned} \tag{A 11}$$

The first term in braces on the right-hand side of (A 11) is the SGS stress tensor. Notice also that $\tilde{u}^r_m = (\tilde{u}^r_m)^r + (\tilde{u}^s_m)^r$, which renders the SGS stress invariant to the extended Galilean group of transformations defined by $x^*_i = x_i + c_i(t)$. Here, we point out that unlike any general filter the wave cut-off filter which is idempotent (i.e. when $\tilde{u}^r_i = (\tilde{u}^r_i)^r$) and has the property that $(\tilde{u}^s_i)^r = 0$, results in the SGS stress for which each term is independently invariant to the extended Galilean group of transformations. Now (A 11) reduces to

$$\tau^*_{ij} = Q_{im}Q_{jn}\tau_{mn} - \left[Q_{im}\dot{Q}_{jn} + \dot{Q}_{in}Q_{jm}\right]\left[x_n\tilde{u}^r_m - (\xi_n\tilde{u}_m)^r\right] - \dot{Q}_{im}\dot{Q}_{jn}\left[x_mx_n - (\xi_m\xi_n)^r\right]. \tag{A 12}$$

When we compare (A 12) to (A 10) we notice that it has additional non-vanishing terms which means that the SGS stress tensor is not frame indifferent.

The sum of the normal components of the second term on the right-hand side of (A 12) is $2\ Q_{im}\dot{Q}_{in}[x_n\tilde{u}^r_m - (\xi_n\tilde{u}_m)^r]$. Notice that $Q_{im}\dot{Q}_{in} = \varepsilon_{inm}\mathscr{W}_i$, where $\mathscr{W}_i$ is the mean intrinsic vorticity related to the rotation rate with respect to an inertial frame of reference and defined as $\mathscr{W}_i = 2\zeta_i + \langle\tilde{\omega}_i\rangle$. Then it follows that the normal stress components due to the second term on the right-hand side of (A 12) are $2\ \mathscr{W}_\alpha\varepsilon_{\alpha nm}[x_n\tilde{u}^r_m - (\xi_n\tilde{u}_m)^r]$ (no summation over Greek indices). These components in general differ from each other, resulting in the normal stress effects. We also notice that the sum of these normal stress components is the dot product of the intrinsic vorticity with the vector difference between the moment of the resolved momentum and the resolved moment of momentum.

By taking the divergence of (A 12) we can examine the effects of the additional terms on the right-hand side of (A 12) on the momentum conservation equation. Using (A 1), (A 2) and since $\partial/\partial x^*_j = Q_{jn}\partial/\partial x_n$ the divergence of (A 12) can be expressed as

$$Q_{im}\frac{\partial\tau_{mn}}{\partial x_n} = \frac{\partial\tau^*_{ij}}{\partial x^*_j} - \varepsilon_{klj}\mathscr{W}_k\left\{(x^*_l - c_l)\frac{\partial\tilde{u}^{*r}_i}{\partial x^*_j} - \left[(\xi^*_l - c_l)\frac{\partial\tilde{u}^*_i}{\partial\xi^*_j}\right]^r\right\}. \tag{A 13}$$

The second term on the right-hand side of (A 13) can be viewed as arising from Coriolis effects.

REFERENCES

Andrén, A., Brown, A. R., Graf, J., Mason, P. J., Moeng, C-H., Nieuwstadt, F. T. M. & Schumann, U. 1994 Large-eddy simulation of a neutrally stratified boundary layer: A comparison of four computer codes. *Q. J. R. Met. Soc.* **120**, 1457–1484.

Bachelor, G. K. 1953 *The Theory of Homogeneous Turbulence*. Cambridge University Press.

Bachelor, G. K. & Townsend, A. A. 1947 Decay of vorticity in isotropic turbulence. *Proc. R. Soc. Lond.* A **199**, 534–550.

Bardina, J., Ferziger, J. H. & Rogallo, R. S. 1985 Effect of rotation on isotropic turbulence: computation and modelling. *J. Fluid Mech.* **154**, 321–336.

Boussinesq, J. 1877 Essai sur la thé des eaux courantes. *Mémoires Preésentés par Divers Savants à l'Académie des Sciences.* **23**.

Businger, J. A., Wyngaard, J. C., Izumi, Y. & Bradley, E. F. 1971 Flux-profile relationships in the atmospheric surface layer. *J. Atmos. Sci.* **28**, 181–189.

Cambon, C., Benoit, J.-P., Shao, L. & Laurent, J. 1994 Stability analysis and large-eddy simulation of rotating turbulence with organized eddies. *J. Fluid Mech.* **278**, 175–200.

Canuto, V. M. & Minotti, F. 1993 Stratified turbulence in the atmosphere and oceans: a new subgrid model. *J. Atmos. Sci.* **50**, 1925–1935.

Champagne, F. H. 1978 The fine-scale structure of the turbulent velocity field. *J. Fluid Mech.* **86**, 67–108.

Coleman, B. D. & Noll, W. 1960 Recent results in the continuum theory of viscoelastic fluids. *Arch. Rat. Mech. Anal.* **3**, 355–370.

De Souza, F. A., Nguyen, V. D. & Tavoularis, S. 1995 The structure of highly sheared turbulence. *J. Fluid Mech.* **303**, 155–167.

Deardorff, J. W. 1970 A numerical study of three-dimensional turbulent channel flow at large Reynolds numbers. *J. Fluid Mech.* **41**, 453–480.

Domaradzki, J. A., Liu, W. & Brachet, M. E. 1993 An analysis of subgrid-scale interactions in numerically simulated isotropic turbulence. *Phys. Fluids* A **5**, 1747–1759.

Dutton, J. A. 1995 *Dynamics of Atmospheric Motion.* Dover.

Foias, C., Manley, O. P. & Temam, R. 1988 Modelling of the interaction of small and large eddies in two dimensional turbulent flows. *Math. Model. Numer. Anal.* **22**, 93–114.

Foias, C., Manley, O. P. & Temam, R. 1991 Approximate inertial manifolds and effective viscosity in turbulent flows. *Phys. Fluids* **3**, 898–911.

Gatski, T. B. & Speziale, C. G. 1993 On explicit algebraic stress models for complex turbulent flows. *J. Fluid Mech.* **254**, 59–78.

Germano, M., Piomelli, U., Moin, P. & Cabot, W. H. 1991 A dynamic subgrid-scale eddy viscosity model. *Phys. Fluids* A **3**, 1760–1770.

Kim, H. T., Klein, S. J. & Reynolds, W. C. 1971 The production of turbulence near a smooth wall in a turbulent boundary layers. *J. Fluid Mech.* **50**, 133–160.

Kolmogorov, A. N. 1941 The local structure of turbulence in incompressible viscous fluid for very large Reynolds' numbers. *Dokl. Akad. Nauk SSSR* **30** (4). Reprinted in *Proc. R. Soc. Lond.* A 1991, **434**, 9–13.

Leigh, D. C. 1962 Non-Newtonian fluids and the second law of thermodynamics. *Phys. Fluids* **5**, 501–502.

Leith, C. E. 1990 Stochastic backscatter in a subgrid-scale model: Plane shear mixing layer. *Phys. Fluids* A **2**, 297–299.

Leslie, D. C. & Quarini, G. L. 1979 The application of turbulence theory to the formulation of subgrid modelling procedures. *J. Fluid Mech.* **91**, 65–91.

Lilly, D. K. 1966 On the application of the eddy viscosity concept in the inertial sub-range of turbulence. *NCAR Manuscript* 123, NCAR, Boulder, CO.

Lilly, D. K. 1967 The representation of small-scale turbulence in numerical experiment. In *Proc. IBM Scientific Computing Symposium on Environmental Sciences. IBM, White Plains, NY.*

Lumley, J. L. 1970 Toward a turbulent constitutive relation. *J. Fluid Mech.* **41**, 413–434.

Lund, T. S. & Novikov, E. A. 1992 Parameterization of subgrid-scale stress by the velocity gradient tensor. In *Annual Research Briefs*, pp. 27–43 Center for Turbulence Research, NASA Ames (Stanford University), Stanford, CA.

Mason, P. J. 1994 Large-eddy simulation: A critical review of the technique. *Q. J. R. Met. Soc.* **120**, 1–35.

Mason, P. J. & Thomson, D. J. 1987 Large-eddy simulations of the neutral-static-stability planetary boundary layer. *Q. J. R. Met. Soc.* **113**, 413–443.

Mason, P. J. & Thomson, D. J. 1992 Stochastic backscatter in large-eddy simulations of boundary layers. *J. Fluid Mech.* **242**, 51–78.

McComb, W. D. 1990 *The Physics of Fluid Turbulence.* Oxford University Press.

Moeng, C.-H. 1984 A large-eddy-simulation model for the study of planetary boundary layer turbulence. *J. Atmos. Sci.* **41**, 2052–2062.

Moeng, C.-H. & Sullivan, P. P. 1994 A comparison of shear- and buoyancy-driven planetary boundary layer flows. *J. Atmos. Sci.* **51**, 999–1022.

Moin, P. & Kim, J. 1982 Numerical investigation of turbulent channel flow. *J. Fluid Mech.* **118**, 341–377.

Piomelli, U., Cabot, W. H., Moin, P. & Lee, S. 1991 Subgrid-scale backscatter in turbulent and transitional flows. *Phys. Fluids* A **3**, 1766–1771.

Piomelli, U., Moin, P. & Ferziger, J. H. 1988 Model consistency in large eddy simulation of turbulent channel flows. *Phys. Fluids* **31**, 1884–1891.

Piomelli, U., Yunfang, Y. & Adrian, R. J. 1996 Subgrid-scale energy transfer and near-wall turbulence structure. *Phys. Fluids* **8**, 215–224.

Pope, S. B. 1975 A more general effective-viscosity hypothesis. *J. Fluid Mech.* **72**, 331–340.

Prandtl, L. 1925 Bericht über Untersuchungen zur ausgebildeten Turbulenz. *Z. Angew. Math. Mech.* **5**, 136–139.

Rivlin, R. S. 1957 The relation between the flow of non-Newtonian fluids and turbulent Newtonian fluids. *J. Rat. Mech. Anal.* **15**, 213–215.

Rivlin, R. S. & Ericksen, J. L. 1955 Stress-deformation relationships for isotropic materials. *J. Rat. Mech. Anal.* **4**, 323–425.

Rogers, M. M. & Moin, P. 1987 The structure of the vorticity field in homogeneous turbulent flows. *J. Fluid Mech.* **176**, 33–66.

Rose, W. G. 1966 Results of an attempt to generate a homogeneous turbulent shear flow. *J. Fluid Mech.* **25**, 97–120.

Rubinstein, R. & Barton, M. J. 1990 Nonlinear Reynolds stress models and the renormalization group. *Phys. Fluids* A **2**, 1472–1476.

Schumann, U. 1975 Subgrid scale model for finite difference simulation of turbulent flows in plane channels and annuli. *J. Comput. Phys.* **18**, 376–404.

Schumann, U. 1995 Stochastic backscatter of turbulence energy and scalar variance by random subgrid-scale fluxes. *Proc. R. Soc. Lond.* A **451**, 293–318.

Serrin, J. 1959 Mathematical principles of classical fluid mechanics. In *Handbuch der Physik*., vol. 8, pp. 126–263.

Smagorinsky, J. 1963 General circulation experiments with the primitive equations. *Mon. Weath. Rev.* **91**, 99–164.

Spencer, A. J. M. & Rivlin, R. S. 1959 The theory of matrix polynomials and its application to the mechanics of isotropic continua. *Arch. Rat. Mech. Anal.* **2**, 309–336.

Speziale, C. G. 1981 Some interesting properties of two-dimensional turbulence. *Phys. Fluids.* **24**, 1425–1427.

Speziale, C. G. 1985 Galilean invariance of subgrid-scale stress models in the large-eddy simulation of turbulence. *J. Fluid Mech.* **156**, 55–62.

Speziale, C. G. 1987 On nonlinear $K - l$ and $K - \epsilon$ models of turbulence. *J. Fluid Mech.* **178**, 459–475.

Speziale, C. G. 1991 Analytical methods for the development of Reyolds-stress closures in turbulence. *Ann. Rev. Fluid Mech.* **23**, 107–157.

Sullivan, P. P., McWilliams, J. C. & Moeng, C.-H. 1994 A subgrid-scale model for large-eddy simulation of planetary boundary-layer flows. *Boundary-Layer Met.* **71**, 247–276.

Tavoularis, S. & Corrsin, S. 1981 Experiments in nearly homogeneous turbulent shear flow with a uniform mean temperature gradient. Part 1. *J. Fluid Mech.* **104**, 311–347.

Tennekes, H. & Lumley, J. L. 1972 *First Course in Turbulence*. The MIT Press.

Truesdell, C. A. 1977 *A First Course In Rational Continuum Mechanics*. Academic.

Truesdell, C. A. & Noll, W. 1965 *The Non-Linear Field Theories of Mechanics*. Springer.

Vreman, B., Geurts, B. & Kuerten, H. 1994 Realizability conditions for the turbulent stress tensor in large-eddy simulation. *J. Fluid Mech.* **278**, 351–362.

Wong, V. C. 1992 A proposed statistical-dynamic closure method for the linear or nonlinear subgrid-scale stresses. *Phys. Fluids* A **4**, 1080–1082.

Wyngaard, J. C. & Tennekes, H. 1970 Measurements of the Small-Scale Structure of Turbulence at Moderate Reynolds Numbers. *Phys. Fluids* **13**, 1962–1969.

Yoshizawa, A. 1984 Statistical analysis of the deviation of the Reynolds stress form its eddy-viscosity representation. *Phys. Fluids* **27**, 1377–1387.